European Journal of Pharmacology 1007 (2025) 178295

Contents lists available at ScienceDirect

European Journal of Pharmacology

journal homepage: www.elsevier.com/locate/ejphar

Improving neuroblastoma therapy with a new p53 family-activating agent

Joana Almeida [a], Diana I.S.P. Resende [b,c,d], Rita Silva [a], Aranzazu Villasante [e,f,g], Catherine Murphy [e], Veronica Zingales [h,i], Andreia Palmeira [c], Jan Škoda [j,k], Francesca Broso [l], Aiswariya Vadivellu [m], Paula Oliveira [n], Salette Reis [o], Cláudia Nunes [o], Amos Hong Pheng Loh [m], Joana M. Ferreira [p,q], Eduarda P. Martins [p,q], Bruno M. Costa [p,q], Alberto Inga [l], Josep Samitier [e,f,g], Emília Sousa [b,c,*], Lucília Saraiva [a,**]

[a] LAQV/REQUIMTE, Laboratório de Microbiologia, Departamento de Ciências Biológicas, Faculdade de Farmácia, Universidade do Porto, 4050-31b, Porto, Portugal
[b] LQOF, Laboratório de Química Orgânica e Farmacêutica, Departamento de Ciências Químicas, Faculdade de Farmácia, Universidade do Porto, Rua de Jorge de Viterbo Ferreira 228, 4050-313, Porto, Portugal
[c] CIIMAR/CIMAR LA, Centro Interdisciplinar de Investigação Marinha e Ambiental, Universidade do Porto, Terminal de Cruzeiros do Porto de Leixões, 4450-208, Matosinhos, Portugal
[d] ICBAS, Instituto de Ciências Biomédicas Abel Salazar, Universidade do Porto, Rua de Jorge de Viterbo Ferreira 228, 4050-313, Porto, Portugal
[e] Institute for Bioengineering of Catalonia (IBEC), The Barcelona Institute of Science and Technology (BIST), 08028, Barcelona, Spain
[f] Department of Electronic and Biomedical Engineering, University of Barcelona, 08028, Barcelona, Spain
[g] Biomedical Research Networking Center in Bioengineering, Biomaterials and Nanomedicine (CIBER-BBN), 28029, Madrid, Spain
[h] Laboratory of Toxicology, Faculty of Pharmacy and Food Science, University of Valencia, Av. Vicent Andrés Estellés s/n, 46100, Valencia, Spain
[i] Department of Industrial Engineering (DII), University of Padua, Fondazione Istituto di Ricerca Pediatrica Città della Speranza (IRP-CdS), Padua, Italy
[j] Department of Experimental Biology, Faculty of Science, Masaryk University, 62500, Brno, Czechia
[k] International Clinical Research Center, St. Anne's University Hospital, 65691, Brno, Czechia
[l] Department of Cellular, Computational and Integrative Biology (CIBIO), University of Trento, Trento, Italy
[m] VIVA-KKH Paediatric Brain and Solid Tumour Programme, Children's Blood and Cancer Centre, KK Women's and Children's Hospital, Singapore, Singapore
[n] Institute for Innovation, Capacity Building and Sustainability of Agri-food Production (Inov4Agro), Centre for Research and Technology of Agro-Environmental and Biological Sciences (CITAB), Vila Real, Portugal
[o] LAQV/REQUIMTE, Departamento de Ciências Químicas, Faculdade de Farmácia, Universidade do Porto, 4050-313, Porto, Portugal
[p] Life and Health Sciences Research Institute (ICVS), School of Medicine, University of Minho, Campus Gualtar, 4710-057 Braga, Portugal
[q] ICVS/3B's - PT Government Associate Laboratory, Braga/Guimarães, Portugal

ARTICLE INFO

Keywords:
Neuroblastoma
p53 family proteins
MDM2
N-Myc
Targeted anticancer therapy
Xanthone derivative

ABSTRACT

Neuroblastoma (NB) is among the most common malignancies in children and represents a therapeutic challenge in pediatric oncology. p53 family proteins play a critical role in protecting cells from genomic instability and malignant transformation. However, in NB, their activities are often inhibited by interacting proteins such as MDM2. The interplay between p53 family pathway and N-Myc, a key biomarker of poor prognosis, is also a critical factor in NB pathogenesis. Herein, we disclose 1-(dibromomethyl)-3,4,6-trimethoxy-9*H*-xanthen-9-one (LEM3) as a new p53 family-activating agent with potent NB anticancer activity. At 0.13–2.1 μM, LEM3 inhibited the growth of several NB cell lines. Its activity was further evidenced in spheroids, patient-derived NB cells, and in a vasculature stiffness-based model of *MYCN*-amplified NB cells. This growth-inhibitory effect was associated with cell cycle arrest and apoptosis, in SH-SY5Y and SK-N-BE(2) NB cells, without apparent acquisition of resistance. LEM3 inhibited cell migration and invasion and reduced the expression of NB-related prognostic markers, particularly *MYCN* mRNA and protein levels. LEM3 released p53, TAp63, and TAp73 from their interaction with MDM2 both in a yeast-based assay and NB cells; for p53, this led to increased protein stabilization, DNA-binding ability, and transcriptional activity. Fluorescence quenching and docking analyses suggested that LEM3 binds to p53, TAp63, and TAp73 at the MDM2-binding site within their transactivation domain. LEM3 also synergies with doxorubicin and cisplatin in NB cells. Given the central role of the p53 family-

* Corresponding author. CIIMAR/CIMAR LA, Centro Interdisciplinar de Investigação Marinha e Ambiental, Universidade do Porto, Terminal de Cruzeiros do Porto de Leixões, 4450-208, Matosinhos, Portugal.
** Corresponding author.
E-mail addresses: esousa@ff.up.pt (E. Sousa), lucilia.saraiva@ff.up.pt (L. Saraiva).

https://doi.org/10.1016/j.ejphar.2025.178295
Received 10 July 2025; Received in revised form 18 October 2025; Accepted 23 October 2025
Available online 24 October 2025

MDM2-*MYCN* axis in NB pathogenesis, our findings support LEM3 as a promising compound for advancing NB targeted therapy.

1. Introduction

Neuroblastoma (NB) is a solid tumor with high prevalence in children under the age of 10, representing 6–10 % of all pediatric malignancies (Shi et al., 2022). NB often forms in areas of the sympathetic nervous system, particularly in the abdomen and adrenal glands (Matthay et al., 2016). The heterogeneity of NB, characterized by multiple chromosomal abnormalities at the genomic level, is regarded as a defining feature of the disease. This makes treatment particularly difficult, especially because of the frequent heterogeneity between and within tumors in patients, as well as the buildup of gene mutations in recurring tumor tissues (Lundberg et al., 2022). Targeted therapy is currently being researched for NB treatment, especially in combination with standard chemotherapy, but the therapeutic success has been limited.

One of the most well-known genetic factors contributing to the development of high-risk NB is *MYCN* amplification (Nakagawara et al., 2018; Nicolai et al., 2015; Park et al., 2010). Abnormal overexpression of the *MYCN* oncogene is linked to increased tumor aggressiveness, resistance to chemotherapy and poor prognosis (Nakagawara et al., 2018; Nicolai et al., 2015; Park et al., 2010). *MYCN* encodes for the protein N-Myc, which directly regulates genes that maintain pluripotency and promote cell proliferation (Otte et al., 2021). The expression of N-Myc is essential for normal neural development. However, although it is active during the development of neural crest cells, N-Myc levels are significantly decreased in fully differentiated adult neural tissue (Chen and Guan, 2022). Numerous clinical studies have shown that *MYCN* amplification is an early event in the development of high-risk NB (Brodeur et al., 1984; Finklestein and Gilchrist, 2010; Huang and Weiss, 2013; Schwab et al., 1983; Seeger et al., 1985).

The p53 family genes, *TP53*, *TP63*, and *TP73*, encode proteins with similar structures that are critical for maintaining genomic integrity and preventing malignant transformation (as reviewed in (Ramos et al., 2020)). The full-length proteins TAp63 and TAp73, which contain the transactivation (TA) domain, act as transcription factors with tumor suppressor properties like p53. In addition, the DNA-binding domains (DBD) of TAp63 and TAp73 share approximately 60–63 % sequence homology with p53, indicating that they may bind to the same DNA sequences and share target genes (Wang et al., 2020). Under normal conditions, the basal levels of p53 family proteins are typically low (Ichimiya et al., 2000; Machado-Silva et al., 2010; Vousden and Lane, 2007).

NB typically carries a wild-type form of p53 (wtp53), which is inactivated through interaction with inhibitory proteins such as MDM2 (as reviewed in (Almeida et al., 2022)). In fact, in many cancers, including NB (Corvi et al., 1995), *MDM2* is overexpressed or amplified, functioning as an oncogene and contributing to therapeutic resistance and metastasis (reviewed in (Zafar et al., 2021)). The inhibition of TAp73 by MDM2 has also been linked to NB, particularly in high-risk and relapsed cases (Zafar et al., 2021). By binding to p53 family proteins, MDM2 can suppress their transcriptional activity. Additionally, MDM2 binds to p53 and functions as an E3 ubiquitin ligase, targeting p53 for degradation by the proteasome. It is important to note that MDM2 is transcriptionally activated by p53, creating a negative feedback loop (Bálint et al., 1999; Dobbelstein et al., 1999). Notably, MDM2 overexpression has been shown to drive drug resistance in wtp53 NB cells by inactivating p53 and TAp73 (Shi et al., 2010). Accordingly, preclinical studies have shown that NB cells are highly sensitive to MDM2 inhibitors, such as nutlin-3a. However, the number of MDM2 inhibitors currently undergoing clinical trials for NB treatment is quite limited (Barbieri et al., 2006; Gamble et al., 2011; Van Maerken et al., 2006).

MYCN amplification plays a key role in the p53-MDM2 pathway (Gu et al., 2011; He et al., 2011). In NB cells, N-Myc directly promotes the transcription of MDM2, which subsequently targets p53 for degradation (Slack et al., 2005). More recently, it was found that N-Myc can directly regulate the p53 transcriptional activity in *MYCN*-amplified NB, by binding to the C-terminal domain of p53, significantly altering the expression of p53 target genes (Agarwal et al., 2018). This interaction with p53 also leads to the activation of alternative p53 targets, further enhancing the oncogenic effects of N-Myc overexpression (Agarwal et al., 2018). By increasing MDM2 levels, N-Myc may also indirectly suppress the TAp73 transcriptional activity (Zhu et al., 2002). Some studies have also indicated that N-Myc overexpression can reduce TAp73 expression by repressing its transcription, in NB cells (Zhu et al., 2002). Conversely, when TAp73 is overexpressed, N-Myc levels are decreased, promoting neuronal differentiation. This suggests an antagonistic relationship between these two transcription factors, influencing NB proliferation and differentiation (Horvilleur et al., 2008; Zhu et al., 2002). MDM2 can also stabilize *MYCN* mRNA and enhance its translation, creating a p53-independent positive feedback loop that drives *MYCN* amplification, promoting the growth and survival of NB cells (Gu et al., 2011). Consistently, NB cells, including p53-null cells with *MYCN* amplification, have shown high sensitivity to MDM2 inhibitors, indicating a p53-independent mechanism of action, primarily through targeting the N-Myc pathway (Gamble et al., 2011; Gu et al., 2011; Van Maerken et al., 2006).

p53 mutations are rare at diagnosis in NB, occurring in less than 2 % of primary tumors, but the frequency increases to around 15 % in relapsed cases (Carr-Wilkinson et al., 2010). Indeed, most clinical cases of mutant p53 (mutp53) in NB are associated with relapse and poor prognosis (Almeida et al., 2022). Despite the loss of p53 functionality in these tumors, the possibility of activating other tumor suppressor members of the p53 family, such as TAp63 and TAp73, emerges as a promising strategy in cases of NB carrying mutp53 (Li and Prives, 2007; Vilgelm et al., 2008).

In this study, we reported the identification of 1-(dibromomethyl)-3,4,6-trimethoxy-9*H*-xanthen-9-one (LEM3; Fig. 1A), and investigated its antitumor potential, both as a standalone treatment and in combination therapy, against NB.

2. Materials and Methods

2.1. Synthesis

2.1.1. Materials and general methods

All reagents and solvents were purchased from TCI, Acros, Sigma Aldrich, or Alfa Aesar and had no further purification process. Solvents were evaporated using a rotary evaporator (Buchi Waterchath B-480) under reduced pressure. Microwave (MW) reactions were performed using an Ethos MicroSYNTH 1600 Microwave Labstation from Milestone. The internal reaction temperature was controlled by a fiber-optic probe sensor. All reactions were monitored by TLC carried out on precoated plates with 0.2-mm thickness using Merck silica gel 60 (GF_{254}) with appropriate mobile phases and detection at 254 and/or 365 nm. Purification of the synthesized compounds was performed by chromatography flash column using Merck silica gel 60 (0.040–0.063 mm). Melting points (m.p.) were measured in a Köfler microscope and are uncorrected. ^{1}H and ^{13}C-NMR spectra were taken in $CDCl_3$ at room temperature on a Bruker Avance 300 instrument (300.13 or 500.13 MHz for ^{1}H- and 75.47 or 125.77 MHz for ^{13}C-). Chemical shifts are expressed in δ (ppm) values relative to tetramethylsilane (TMS) as an internal

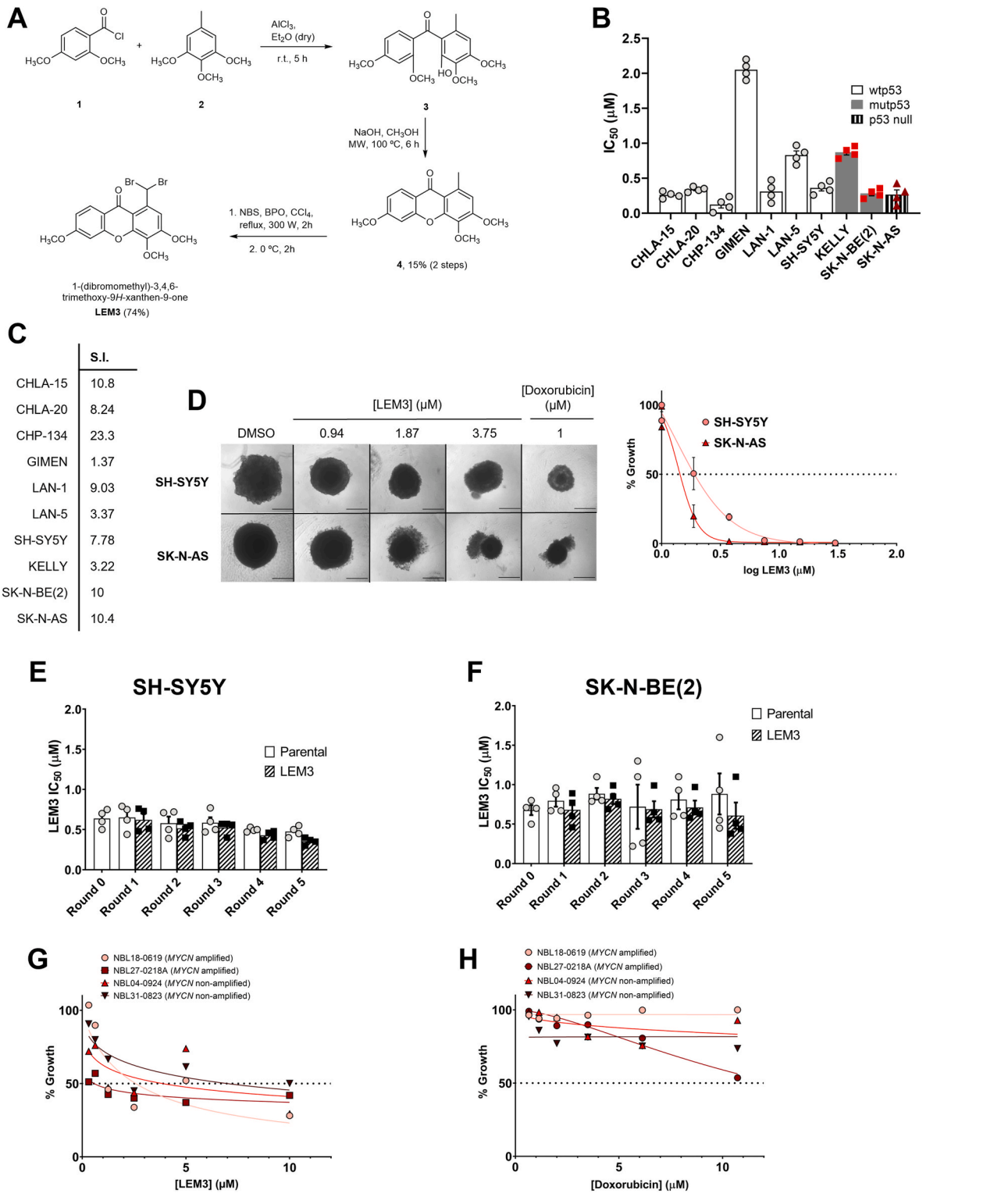

Fig. 1. LEM3 suppresses NB cell growth without promoting drug resistance. (**A**) Synthesis of 1-(dibromomethyl)-3,4,6-trimethoxy-9*H*-xanthen-9-one (**LEM3**). (**B**) IC_{50} values of LEM3 in NB cell lines, determined by MTT assay, after 48 h of treatment. Data are mean ± SD (n = 4). (**C**) Selectivity indexes for NB cells relative to the normal fibroblast HFF-1 cell line, in which LEM3 had an IC_{50} of 2.8 μM. (**D**) Brightfield imaging of SH-SY5Y and SK-N-AS spheroids, treated with LEM3 or solvent for 7 days. Spheroids were seeded in the presence of LEM3, doxorubicin, or solvent. Images are representative of 4 independent experiments; scale bar = 500 μm; magnification = 40 × . Dose-response curves for the growth inhibitory activity of 0.94–30 μM of LEM3 on 7-day old SH-SY5Y and SK-N-AS spheroids, determined using CellTiter-Glo® 3D Cell Viability Assay (n = 4; 6 replicates per condition and per experiment). (**E**, **F**) LEM3-induced resistance in NB cells. SH-SY5Y and SK-N-BE (2) cells were exposed to five rounds of treatment with LEM3 (0.06, 0.09, 0.12, 0.15 and 0.20 μM for SH-SY5Y (**E**); 0.05, 0.07, 0.09, 0.12 and 0.15 μM for SK-N-BE(2) (**F**)). IC_{50} values were determined at the end of each round by MTT assay after 48 h of treatment. Data were normalized to DMSO and correspond to mean ± SD (n = 4; two replicates each); values not significantly different from parental cells: $p > 0.05$, two-way ANOVA followed by Sidak's test. (**G**, **H**) Dose-response curves for the growth inhibitory activity of (**G**) 0.31–10 μM of LEM3 and (**H**) 0.65–10.7 μM of doxorubicin, in NB primary cell lines, determined by MTT assay, after 72 h of treatment. Data are mean ± SD (n = 4).

reference. Coupling constants are reported in hertz (Hz). ^{13}C-NMR assignments were made by 2D HSQC and HMBC experiments (long range C, H coupling constants were optimized to 7 and 1 Hz). HRMS mass spectra were measured on a Bruker Daltonics micrOTOF Mass Spectrometer, recording in ESI (electrospray) mode in Centro de Apoio Científico e Tecnolóxico á Investigation (C.A.C.T.I.), University of Vigo, Galicia, Spain.

2.1.2. Synthesis of 3,4,6-trimethoxy-1-methyl-9H-xanthen-9-one (4)

3,4,6-trimethoxy-1-methyl-9*H*-xanthen-9-one (**4**) was prepared by previously established methodologies, and its structural characterization data aligned with prior descriptions (Resende et al., 2018, 2020b).

2.1.3. Synthesis of 1-(dibromomethyl)-3,4,6-trimethoxy-9H-xanthen-9-one (LEM3)

A mixture of 3,4,6-trimethoxy-1-methyl-9*H*-xanthen-9-one (0.629 g, 2.095 mmol), *N*-bromosuccinimide (0.746 g, 4.190 mmol) and dibenzoylperoxide (0.152 g, 0.628 mmol) in carbon tetrachloride (12 mL) was refluxed for 2 h under light (300 W). After cooling at 0 °C and stirring for 2 h, the precipitate was filtered and washed with cold carbon tetrachloride. The mother liquor was evaporated under reduced pressure and purified by flash chromatography (silica gel, petroleum ether/ethyl acetate 9:1) to obtain the pure product (purity >95 %, Supplementary Material Figs. S1–S3) 1-(dibromomethyl)-3,4,6-trimethoxy-9*H*-xanthen-9-one (LEM3, 0.320 g, 72 % yield) as white needles (0.71 g, 74 %); m.p. 159–161 °C. ^{1}H-NMR ($CDCl_3$, 300.13 MHz): δ = 8.98 (s, 1H, H-1′), 8.20 (d, $^{3}J_{8,7}$ = 7.9 Hz, $^{4}J_{8,5}$ = 1.3 Hz, 1H, H-8), 7.74 (1H, s, H-2), 6.97–6.92 (m, 2H, H-5, H-7), 4.10 (3H, s, 3-OCH_3), 4.04 (3H, s, 4-OCH_3), 3.95 (3H, s, 6-OCH_3) ppm. ^{13}C-NMR ($CDCl_3$, 75.47 MHz): δ = 177.1 (C-9), 165.4 (C-6), 157.0 (C-10a), 156.3 (C-3), 150.5 (C-4a), 139.6 (C-1), 137.6 (C-4), 128.6 (C-8), 116.1 (C-8a), 114.0 (C-7), 111.9 (C-2), 111.0 (C-9a), 99.8 (C-5), 61.8 (4-OCH_3), 56.7 (3-OCH_3), 56.1 (6-OCH_3), 39.5 (C-1′) ppm. HRMS (ESI^+): *m/z* $[C_{17}H_{14}Br_2O_5 + H]^+$ calcd. for $[C_{17}H_{15}Br_2O_5]$: 456.9281; found 456.9275.

2.2. Chemicals preparation

Doxorubicin, (Sigma-Aldrich, Portugal), 13cisRA (R3255, Sigma-Aldrich) and LEM3 were dissolved in DMSO (Sigma-Aldrich). Cisplatin (Enzo Life Sciences, Taper, Portugal) was dissolved in saline. In all experiments, the solvent was included as a control at a concentration that did not affect cell proliferation (maximum concentration used of 0.1 %). Doxorubicin (Pfizer) was diluted from its original stock solution of 50 mg/25 mL to the required concentrations.

2.3. Cell cultures

The following established neuroblastoma cell lines were used in the study: (i) *MYC*-amplified CHLA-15 and CHLA-20 (obtained from the COG/ALSF Childhood Cancer Repository and kindly provided by Prof. Michael D. Hogarty, Children's Hospital of Philadelphia, PA, USA), (ii) *MYCN*-amplified LAN-1, LAN-5, KELLY (a kind gift of Prof. Lumír Krejčí, Masaryk University, Brno, Czech Republic) and SK-N-BE(2) (purchased from ECACC), and (iii) *MYCN/MYC*-non amplified GIMEN (a kind gift of Prof. Lumír Krejčí) and SH-SY5Y (purchased from ECACC). *MYCN*-amplified CHP-134 and *MYCN*-non amplified SK-N-AS cells were kindly provided by Prof. Alessandro Quattrone (CIBIO, University of Trento, Italy). All cell lines were passaged between 10 and 15 times. CHLA-15, CHLA-20 and GIMEN cell lines were cultured in DMEM-F12 with 10 % FBS, 2 mM L-glutamine, 100 IU/mL penicillin, 100 μg/mL streptomycin, 1 % NEAA and 0.12 % ITS-X. KELLY, LAN-1 and LAN-5 cells were cultured in RPMI with 10 % FBS, 2 mM L-glutamine, 100 IU/mL penicillin and 100 μg/mL streptomycin. SH-SY5Y cells were cultured in DMEM-F12 with 20 % FBS, 2 mM L-glutamine, 100 IU/mL penicillin and 100 μg/mL streptomycin. CHP-134 and SK-N-BE(2) cell lines were cultured in RPMI with 10 % FBS, 2 mM L-glutamine, 100 IU/mL penicillin and 100 μg/mL streptomycin. SK-N-AS cells were cultured in DMEM with 10 % FBS, 2 mM L-glutamine, 100 IU/mL penicillin and 100 μg/mL streptomycin. All cell lines were grown at 37 °C with 5 % CO_2. All supplements were obtained from Gibco, Thermo Fisher Scientific - US.

2.4. MTT (3-(4, 5-dimethylthiazolyl-2)-2, 5-diphenyltetrazolium bromide) assay

Cells were seeded in 96-well plates at 5×10^3 (CHLA-15, CHLA-20, GIMEN, LAN-1, LAN-5 and KELLY) and 7.5×10^3 (CHP-134, SH-SY5Y, SK-N-AS and SK-N-BE(2)) cells/well and the half maximal inhibitory concentration (IC_{50}) values of compounds were determined as described (Gomes et al., 2019).

2.5. Spheroids generation

SH-SY5Y and SK-N-AS cells were seeded in Corning® ULA 96-well round-bottom plates (New York, USA) at a density of 2×10^3 cells/well, as performed in (Zingales et al., 2024). For SK-N-AS cells, 3 μg/mL of collagen I was also added at the time of seeding. SK-N-AS and SH-SY5Y spheroids were cultured for 7 days, with medium replenishment on day 4 only for the latter. After 7 days of growth, 100 μL of the culture medium per well was replaced with 100 μL of medium containing a 2X concentration of treatment, to reach the target concentration in the well. At the end of the exposure time, the CellTiter-Glo 3D Cell Viability Assay was conducted according to the manufacturer's instructions (Zingales et al., 2024).

2.6. Annexin-V assay

SH-SY5Y and SK-N-BE(2) (2.25×10^5 cells/well) were seeded in 6-well plates, followed by treatment for 48 h with 0.4 and 0.8 μM (SH-SY5Y) or 0.3 and 0.6 μM (SK-N-BE(2)) of LEM3. For detection of apoptotic cell death, the Annexin V-FITC Apoptosis Detection Kit I (BD Biosciences) was used according to the manufacturer's instructions. The Accuri cytometer and the BD Accuri C6 software were used (BD Biosciences, Enzifarma, Portugal).

2.7. Cell cycle analysis

SH-SY5Y and SK-N-BE(2) were seeded in 6-well plates (2.25×10^5 cells/well), followed by treatment for 48 h with 0.4 and 0.8 μM (SH-SY5Y) or 0.3 and 0.6 μM (SK-N-BE(2)) of LEM3. Cells were collected and stained with propidium iodine, followed by flow cytometry analysis using Accuri TM C6 flow cytometer and the BD Accuri C6 software (BD Biosciences, Enzifarma, Portugal). Cell cycle phases were identified and quantified using the FlowJo X 10.0.7 Software (Treestar, Ashland, OR, USA).

2.8. Acquired resistance studies

SH-SY5Y and SK-N-BE(2) cells were exposed to five rounds of selection with increasing concentrations of LEM3 (0.06, 0.09, 0.12, 0.15 and 0.20 μM for SH-SY5Y; 0.05, 0.07, 0.09, 0.12 and 0.15 μM for SK-N-BE(2)), which were added to the culture medium for 24 h, followed by a recovery time of 48 h in fresh medium without treatment. This procedure was previously used to generate doxorubicin-resistant cells (Raimundo et al., 2018). Cells were harvested, seeded, and treated twice for each concentration (one round). The same passage number of both parental and resistant cells was used in the experiment. At the end of each round, IC_{50} values were determined by MTT assay, after 48 h of treatment.

2.9. Western blot

SH-SY5Y and SK-N-BE(2) were seeded in 6-well plates (2.25×10^5 cells/well), followed by treatment for 48 h with 0.4 and 0.8 μM (SH-SY5Y) or 0.3 and 0.6 μM (SK-N-BE(2) of LEM3 for 48 h, and were collected for protein extraction. Protein extracts were quantified using the Bradford reagent (Sigma-Aldrich). Proteins were run in SDS-PAGE and transferred to a Whatman nitrocellulose membrane (Amersham Protran, Germany). Membranes were blocked in 5 % low-fat milk and labeled with specific primary antibodies followed by HRP-conjugated secondary antibodies (Supplementary Table S1). For signal detection, the ECL Prime Amersham kit (GE Healthcare, VWR) and ChemiDoc™ MP Imaging System (Bio-Rad Laboratories, Portugal) were used. Antibodies are listed in Supplementary Table S1.

2.10. TransAM assay

SH-SY5Y cells were seeded in 6-well plates (2.25×10^5 cells/well). Cells were thereafter treated with IC_{50} and $2 \times IC_{50}$ concentration of LEM3 (or DMSO only) for 24 h. Nuclear protein extracts were obtained using the Nuclear Extract Kit from Active Motif, and the protein concentration was measured using NanoDrop 1000 from Thermo Scientific. The p53 DNA binding ability was evaluated using the TransAM p53 Transcription Factor Assay Kit from Active Motif, according to the manufacturer's instructions. Briefly, equal amount of total nuclear protein was loaded into a 96-well plate coated with an immobilized oligonucleotide containing a p53 consensus binding site. The amount of bound p53 protein was quantified using an anti-p53 antibody followed by a HRP-conjugated secondary antibody. The HRP signal was measured after addition of a manufacturer's substrate, using the Bio-Tek Synergy HT plate reader at 450 nm.

2.11. RT-qPCR

SH-SY5Y and SK-N-BE(2) cells were seeded in ⌀100 mm petri dishes at 1.5×10^6 cells/dish, followed by treatment with LEM3, 13-cis-retinoic acid (13cisRA) or solvent. Total RNA was extracted using NucleoSpin® RNA Kit (Macherey-Nagel GmbH & Co. KG, Germany). One μg of RNA was used for cDNA synthesis using the RevertAid cDNA Synthesis kit (Thermo Fisher Scientific) in 20 μL final volume, following manufacturer's instructions. RT-qPCR was performed in a 384-well plate on an Applied Systems Life QuantStudio 5384 RT-PCR system (Thermo Fisher Scientific). The PowerUp™ SYBR™ Green Master Mix for qPCR was used. The relative mRNA expression levels were determined using the ΔΔCt method. The expression levels of the target genes were normalized to the reference gene *GAPDH* and calibrated to the DMSO-treated control sample. Primer sequences are listed in Supplementary Table S2.

2.12. Yeast-based assay

Saccharomyces cerevisiae cells expressing human p53, TAp63α or TAp73α alone or co-expressed with human MDM2, and transformed with respective empty vectors (control); pLS89-(*TRP1*)-*GAL1-10* encoding human p53, pTSG-(*TRP1*)-*GAL1-10* encoding TAp63α, pRS314-(*TRP1*)-*GAL1-10* encoding TAp73α and pGADT7-(*LEU2*)-*GAL1-10* encoding human MDM2, were previously obtained (Leão et al., 2015). Yeast screening assay was established by measuring the growth of yeast cells as described (Leão et al., 2015). Briefly, cells were grown in galactose-selective medium with compounds or 0.1 % DMSO for 48 h; cell growth was analyzed by colony-forming unit counts.

2.13. Co-immunoprecipitation (Co-IP) assay

Co-IP was performed using the Pierce Classic Magnetic IP and Co-IP Kit (Thermo Scientific, Dagma, Portugal), according to manufacturer's instructions (Soares et al., 2017). p53, TAp63, TAp73, MDM2 were detected by Western blot; GAPDH was used as a loading control.

2.14. Cycloheximide (CHX) assay

SH-SY5Y cells were seeded in 6-well plates at 2.3×10^5 cells/well for 24 h, followed by 24 h of treatment with 0.4 μM of LEM3 or solvent. Thereafter, cells were treated with 150 μg/mL of CHX (Sigma-Aldrich) for 0, 0.5, 1, 1.5, and 2 h p53 protein expression was detected by Western blot; GAPDH was used as a loading control.

2.15. Protein-ligand interaction by fluorescence quenching

Evaluation of the potential binding of LEM3 to recombinant human p53 (Millipore/Merck, CA, USA), TAp63α and TAp73α (Sigma-Aldrich, MO, USA) was based on the quenching of the intrinsic fluorescence of the protein. Phosphate buffer, consisting of 50 mM HEPES, 5 mM DTT, 10 mM Zn $(CH_3CO_2)_2$, and 150 mM NaCl (pH 7.5), was used in the preparation of all solutions. Briefly, 5 mM of each protein, increasing concentrations of drug solution (0–75 mM) and phosphate buffer solution (pH 7.5) were mixed to a final volume of 280 μL. Fluorescence emission spectra were recorded at room temperature (25 ± 1 °C) in a microplate reader (Synergy HT Multi-Detection Microplate Reader, BioTek, Izasa Scientific) in the range of 300–350 nm upon excitation at 280 nm. Protein-LEM3 binding parameters were calculated using the Origin 8.5.1 software v8.5.1 (OriginLab Corporation, Northampton, MA, USA). The fitting of the experimental values was made according to the Langmuir binding equation. The protein binding parameters of the interaction monitored by fluorescence were calculated through the fitting of the experimental points of the following equation (adapted from (Fernandes et al., 2017)):

$$[protein - LEM3] = Quenching\ (\%) = \frac{y_{max}^{n}}{1 + \frac{K_d}{[LEM3]}}$$

where y_{max} corresponds to the highest quenching induced by LEM3, n accounts for the number of binding sites, and Kd corresponds to the dissociation constant of protein-LEM3 complexes.

2.16. In silico analysis

ADME prediction: LEM3 was evaluated through SwissADME to predict oral absorption (Lipinski's rule of five (RO5)) and blood-brain barrier (BBB) permeability.

Docking: The 3D structures of LEM3 were drawn using Hyperchem 7.5 (Hypercube, FL, USA), being minimized by the semi-empirical Polak-Ribiere conjugate gradient method (RMS<0.1 kcal $Å^{-1}.mol^{-1}$). Crystal structure of TA domain of p53 (PDB code: 1ycr), TAp63 (PDB code: 6fgn) and TAp73 (PDB code: 2mps) were downloaded from the protein databank (PDB). Additional structures included in the pdb files, such as MDM2 or p300, were excluded. Hydrogen atoms were added to the protein structure and gasteiger charges were computed. The protein-ligand docking protocol was performed using a flexible docking approach to account for conformational changes in the binding site residues during ligand binding. Three key residues in the binding site, identified based on their potential for interaction with MDM2 (phenylalanine, tryptophane and leucine), were selected for flexibility. These residues were Phe19, Trp23, and Leu26 in p53; Phe55, Trp59, and Leu62 in TAp63; and Phe15, Trp19, and Leu22 in TAp73. The flexible residues were prepared using Autodocktools 1.5.7. Docking simulations between the target protein and LEM3 was undertaken in AutoDock Vina (Scripps Research Institute, USA) (Jaghoori et al., 2016). The dimensions of the grid box were set to $25 \times 20 \times 25$ Å to engulf the flexible residues and to allow sufficient space for ligand sampling. The exhaustiveness parameter was set to 25 to ensure thorough sampling of ligand conformations. Nine binding poses were sampled and ranked based on

their predicted binding affinities (kcal.mol^{-1}). A postdocking analysis of the top pose on each target was conducted using Pymol 1.3 (Seeliger and De Groot, 2010).

2.17. In vitro migration and invasion assays

For NB cell migration analysis, both the wound-healing assay and the QCM 24-Well Fluorometric Chemotaxis Cell Migration Kit (8 μm) from Merck Millipore (Taper) were used (Soares et al., 2016). Briefly, for the wound-healing assay, 2.25 × 10^5 SH-SY5Y cells/well were grown to confluence in six-well plates, and a fixed width wound was created in the cell monolayer using a sterile 10 μL micropipette tip. Cells were treated with LEM3 at 0.12 and 0.18 μM; images of the wound were captured at consecutive time points using an inverted Nikon TE 2000-U microscope from Nikon Instruments Inc. (Izasa) at 100 × magnification with a DXM1200F digital camera (Nikon Instruments Inc.) and NIS-Elements microscope imaging software (version 4; Nikon Instruments Inc.). For calculation of the wound closure, the subtraction of the "wound" area (measured using ImageJ Software) at the indicated time point of treatment to the "wound" area at the starting point was made. For the chemotaxis cell migration assay and fluorimetric cell invasion assay, 1.2 × 10^5 cells of SH-SY5Y and SK-N-BE(2) (cultured in serum-free medium for 24 h) were prepared for each tested condition. Cells were treated with 0.13 μM of LEM3. The prepared cell suspensions were distributed in 24-well plates (300 μL per insert), followed by an addition of 500 μL medium containing 10 % FBS to the lower chamber. After 24 h, cells that migrated or invaded through the ECMatrix™ layer (with 8 μm pore membranes) were eluted, lysed and stained with a green-fluorescence dye that binds to cellular nucleic acids. The number of migrating/invading cells was proportional to the fluorescence signal measured using the Bio-Tek Synergy HT plate reader (Izasa), at 480/520 nm (ex/em).

2.18. Combination therapy assay

For the assessment of synergistic effects of LEM3 with standard chemotherapeutic agents, SH-SY5Y and SK-N-BE(2) cells were treated with 0.13 and 0.18 μM of LEM3 (for SH-SY5Y) or 0.09 and 0.13 μM of LEM3 (for SK-N-BE(2)) and increasing concentrations of cisplatin (0.5–8 μM) or doxorubicin (6.25–100 nM) for 48 h. The MTT assay was used to assess the effect of the combined treatments on cell proliferation. For each combination, the combination index (C.I.) and the dose reduction index (D.R.I.) values were calculated using the CompuSyn Software version 1.0 (ComboSyn, Inc., Paramus, NJ, USA) according to the following equation: CI = (D)1/(Dx)1 + (D)2/(Dx)2, where the numerators (D)1 and (D)2 are the concentrations of each drug in the combination [(D)1 + (D)2] that inhibit x%, and the denominators (Dx)1 and (Dx)2 are the concentrations of drug one and two alone that inhibit x%; D.R.I. measures how much the dose of a drug may be reduced in synergistic combination compared to the dose of each drug alone; C.I. values < 1, 1 < C.I. < 1.1 and >1.1 indicate synergistic, additive and antagonistic effects, respectively (Chou and Talalay, 1984).

For the 3D spheroid model, SH-SY5Y cells were seeded in Corning® ULA 96-well round-bottom plates (New York, USA) at a density of 2 × 10^3 cells/well, as in (Zingales et al., 2024). The same procedure was followed as for the treatment with LEM3 alone, except cells were treated with 0.8 or 0.35 μM of LEM3 and increasing concentrations of cisplatin (0.5–8 μM) for 48 h. The CellTiter-Glo 3D Cell Viability Assay was conducted according to the manufacturer's instructions.

2.19. Stiffness-based model assay

KELLY cells were cultured and seeded at a density of 25,000 cells/mL on stiffness-tunable substrates previously fabricated as described in (Villasante et al., 2024). For viability and proliferation assays, cells were seeded at 50,000 cells/well on standard tissue culture plastic or on 100 kPa stiffness substrates. After seven days of culture, cells were treated with vehicle (DMSO), 1 μM, or 2 μM of LEM3 for 72 h.

Following treatment, cells were rinsed with phosphate-buffered saline (PBS), trypsinized, and counted manually using a hemocytometer. For live/dead viability analysis, cells were exposed to the same LEM3 treatment conditions. At each time point, samples were incubated in RPMI medium containing 2 μM Calcein-AM and 4 μM Ethidium Homodimer-1 for 30 min at 37 °C and 5 % CO_2, according to the manufacturer's protocol (LIVE/DEAD® Viability/Cytotoxicity Kit, Molecular Probes, Eugene, OR, USA). Nuclear counterstaining was performed using Hoechst 33342 (1 μg/mL, 15 min).

Samples were imaged using an Olympus IX81 fluorescence microscope (Olympus, Center Valley, PA, USA) at 10 × magnification. Images were acquired in brightfield and red, green, and blue fluorescence channels to visualize dead cells, live cells, and nuclei, respectively. Quantification of positively stained cells was performed using the 3D Object Counter plugin in ImageJ (NIH, Bethesda, MD, USA).

2.20. Patient-derived NB cells

Following informed consent under an institutional review board-approved protocol (SHS/2014/2079), NB patients at KK Women's and Children's Hospital were prospectively recruited, and leftover tumor tissue from surgical excisions were used to establish patient-derived cell cultures (PDCs), as previously described (Hee et al., 2020). PDCs (expressing wild-type p53) were subcultured at a 1:2 split ratio from the respective growth densities of each PDC line and seeded in 96-well plates with 135 μL media containing 250 nM IncuCyte® Cytotox Red reagent (Essen Biosciences, Cat 4632) and 15 μL of doxorubicin or LEM3. The range of *in vitro* concentrations of doxorubicin covered the maximum human serum concentrations (Cmax) of doses used in routine upfront clinical protocols (Cheung et al., 2001).

2.21. Statistical analysis

Data were statistically analyzed using GraphPad Prism. Different statistical tests were used depending on the datasets, as indicated in the figure legends; p values < 0.05 were considered statistically significant.

3. Results

3.1. Chemistry

LEM3 was prepared via previously described methods (Fig. 1A) (Resende et al., 2020b). Friedel-Crafts acylation of 1,2,3-trimethoxy-5--methylbenzene (**3**) by 2,4-dimethoxybenzoyl chloride (1), using aluminum chloride as an acid catalyst, gives the benzophenone intermediate **3**. Further nucleophilic addition followed by elimination of methanol under basic conditions and microwave irradiation produced 3, 4-dimethoxy-1-methyl-9*H*-xanthen-9-one (**4**). Subsequent Vohl-Ziegler bromination of this intermediate with brominating agent *N*-bromosuccinimide (NBS) and benzoyl peroxide (BPO) as the radical initiator afforded 1-(dibromomethyl)-3,4,6-trimethoxy-9*H*-xanthen-9-one (**LEM3**) in good yield.

3.2. LEM3 inhibits the growth of NB cells, in 2D and 3D models, without apparent induction of resistance

The growth inhibitory effect of LEM3 was investigated through the MTT assay, in a panel of NB cell lines expressing wtp53 (CHLA-15, CHLA-20, CHP-134, GIMEN, LAN-1, LAN-5, and SH-SY5Y) or mutp53 (KELLY and SK-N-BE(2)), and in p53-null cells (SK-N-AS) (sources: Cellosaurus (Cell Line Knowledge Resource) – https://cellosaurus.org - COSMIC (Catalogue of Somatic Mutations in Cancer) - https://cancer.sanger.ac.uk/cell_lines - DepMap (Cancer Dependency Map) - https://depmap.org/portal/- and The TP53 Database - https://tp53.cancer.

gov/) (Fig. 1B). The results revealed a potent antiproliferative effect of LEM3 in NB cells (IC_{50} values ranging from 0.13 to 2.1 μM; Fig. 1B). Interestingly, GIMEN cells have been reported to exhibit alterations in *TP53*-pathway regulators, namely reduced $p14^{ARF}$ expression, which can impair p53/TAp73 activity and may contribute to their relatively lower sensitivity to LEM3 (Almeida et al., 2022; Carr et al., 2006). In addition, except for GIMEN cells, LEM3 demonstrated an evident selectivity towards NB cells, exhibiting selective indices ranging from 3 to 23 times higher compared to the normal fibroblast HFF-1 cell line (in which LEM3 presented an IC_{50} value of 2.8 μM) (Fig. 1C). Consistently, an effective growth inhibitory effect of LEM3 was also observed in 3D models of NB cells (Fig. 1D). In fact, a marked reduction in spheroids growth was obtained with LEM3, in wtp53-expressing SH-SY5Y (IC_{50} of 1.75 ± 0.34 μM) and p53-null SK-N-AS (IC_{50} of 1.01 ± 0.11 μM) cells.

Despite the existence of several therapeutic strategies for treating NB, long-term resistance often develops, resulting in treatment failure (Zhou et al., 2023). Hence, it is of utmost importance to address this issue in NB treatment. As such, we further evaluated whether NB cells acquired resistance to LEM3, using a protocol previously established to generate drug-resistant cancer cells, namely to doxorubicin (Raimundo et al., 2018). In our experimental conditions, LEM3 did not induce resistance in SH-SY5Y (Fig. 1E) nor SK-N-BE(2) (Fig. 1F) cells, as shown by the maintenance of its IC_{50} values during the several rounds of treatment with increasing concentrations of LEM3.

To further validate the anticancer potential of LEM3 against NB, the activity of the compound was also evaluated in patient-derived NB cells with both amplified (NBL18-0619 and NBL27-0218A cells) and non-amplified (NBL04-0924 and NBL31-0823 cells) *MYCN*. In NBL18-0619 and NBL27-0218A cells, LEM3 showed IC_{50} values of 2.58 ± 0.41 μM and 0.58 ± 0.16 μM, respectively, while its effectiveness was somewhat reduced in NBL04-0924 and NBL31-0823 cells, with IC_{50} values of 3.88 ± 0.59 μM and 7.00 ± 0.84 μM, respectively (Fig. 1G). These findings are noteworthy, as all four patient-derived NB cell lines demonstrated insensibility to doxorubicin, with IC_{50} values above 10 μM (Fig. 1H). Collectively, in a setting that more closely reflects clinical conditions, these results highlighted the efficacy of LEM3 in the context of poor response to standard chemotherapy and N-Myc amplification.

3.3. LEM3 activates p53 family proteins, inducing cell cycle arrest and apoptosis

To further understand the underlying mechanism of action of LEM3, we focused on SH-SY5Y and SK-N-BE(2) cell lines, which express wtp53 and mutp53, respectively. Moreover, SH-SY5Y expresses a mutant form of ALK (F1174L), while SK-N-BE(2) displays *MYCN* amplification, which are both poor prognosis markers. Firstly, we assessed the effect of LEM3 on cell cycle progression. At twice the IC_{50} ($2 \times IC_{50}$) value and 24 h of treatment, while only a modest arrest in the G0/G1 phase was observed in SH-SY5Y cells, LEM3 led to a prominent G2/M phase arrest in SK-N-BE(2) cells (Fig. 2A). The IC_{50} and $2 \times IC_{50}$ values (0.4 and 0.8 μM) of LEM3 markedly increased the percentage of Annexin V-positive cells in SH-SY5Y, while a modest enhancement of apoptotic cells was achieved with the $2 \times IC_{50}$ value (0.6 μM) of LEM3 in SK-N-BE(2) cells (Fig. 2B). It is worth noting that in SK-N-AS cells (p53-null, *MYCN* non-amplified), LEM3 significantly increased G2/M-phase cell cycle arrest and the percentage of Annexin-V–positive cells (Supplementary Fig. S4), providing further evidence that LEM3 retains its capacity to induce apoptosis and cell cycle arrest even in the absence of p53.

In line with the flow cytometry findings, the IC_{50} and $2 \times IC_{50}$ concentrations of LEM3 increased the expression levels of the cell cycle regulator p21, in both SH-SY5Y (Fig. 2C) and SK-N-BE(2) (Fig. 2D) cells. Moreover, in accordance with the induction of apoptotic cell death, LEM3 treatment increased cleaved PARP and caspase-3 levels, as well as pro-apoptotic markers such as PUMA. Additionally, there was a notable downregulation of the anti-apoptotic proteins Bcl-2 and survivin in both cell lines (Fig. 2C and D). Importantly, we detected a marked increase in the protein levels of the tumor suppressors p53, TAp63, and TAp73 in SH-SY5Y cells (Fig. 2C) and TAp63 and TAp73 in SK-N-BE(2) cells (Fig. 2D).

Supporting an activation of wtp53, LEM3 enhanced the DNA-binding ability of p53, in SH-SY5Y cells, as demonstrated by the significant increase in the amount of p53 bound to DNA in the TransAM assay (Fig. 2E). Accordingly, we observed an increase in the mRNA levels of the p53 transcriptional targets *BBC3* (PUMA) and *CDKN1A* (p21), in SH-SY5Y cells treated with 0.4 and 0.8 μM of LEM3 (Fig. 2F), which was consistent with the observed upregulation at protein levels for those and other p53 targets, such as PUMA and MDM2 (Fig. 2C). However, considering the observed augmentation in MDM2, p21, and PUMA protein levels also in the SK-N-BE(2) cells harboring mutp53, we hypothesized that LEM3 may also activate other members of the p53 family, namely TAp63 and TAp73, which play a role in the transcription of p53 target genes.

3.4. LEM3 disrupts the MDM2 interaction with p53 family proteins

Interestingly, it was observed that LEM3 was able to induce p53 stabilization, enhancing p53 half-life upon inhibition of protein synthesis by cycloheximide (CHX) (Fig. 2G). This indicated that LEM3 could prevent p53 from undergoing ubiquitin-mediated degradation by disrupting its binding to MDM2. Although we could not confirm a comparable effect for TAp63 and TAp73, it has been proposed that MDM2-mediated ubiquitination of these proteins does not effectively target them for substantial proteasomal degradation (Armstrong et al., 2016; Osterburg and Dötsch, 2022; Stindt et al., 2014). We then checked whether the potential activation of p53 family proteins by LEM3 could be mediated by their release from MDM2 binding.

To assess this, we first used a yeast-based functional assay previously established to search for potential inhibitors of the MDM2 interaction with p53, TAp63 or TAp73 (Leão et al., 2015). Briefly, in this assay, the expression of p53, TAp63 or TAp73 in yeast induces growth arrest, which is abolished by co-expression of the negative regulator MDM2. Potential inhibitors of the interaction of p53 family proteins with MDM2 should restore the p53 family-induced growth arrest. In this cell system, LEM3 caused a dose-dependent growth inhibition in yeast cells co-expressing MDM2 with p53, TAp63 or TAp73. Instead, no interference with the growth of control yeast or yeast expressing p53, TAp63, TAp73, or MDM2 alone (Fig. 3A–C) was observed. These results suggested an inhibition of the MDM2 interaction with p53, TAp63 and TAp73 by LEM3.

To confirm these results, co-immunoprecipitation assays were performed, in both SH-SY5Y and SK-N-BE(2) NB cells upon 16 h of treatment with LEM3. Of note, the higher doses of LEM3 used in these experiments ($2 \times IC_{50}$ and $3 \times IC_{50}$ values) were chosen in consideration of the shorter incubation time with the compound, which was limited to 16 h. In SH-SY5Y cells, it was observed that 0.8 and 1.2 μM of LEM3 significantly reduced the amount of MDM2 immunoprecipitated with p53 (Fig. 3D), as well as TAp63 (Fig. 3E) and TAp73 (Fig. 3F) immunoprecipitated with MDM2. In line with this, in SK-N-BE(2) cells, 0.6 and 0.9 μM of LEM3 also decreased the amount of TAp63 (Fig. 3G) and TAp73 (Fig. 3H) immunoprecipitated with MDM2.

3.5. LEM3 potentially binds to p53 family proteins

We next investigated the ability of LEM3 to bind to p53, TAp63 and TAp73 proteins. For that, a fluorescence quenching assay, using p53, TAp63, and TAp73 recombinant proteins was performed. This assay measures the quenching of the intrinsic fluorescence of tryptophan residues of a protein that may result from changes in the local environment polarity after the addition of a potential ligand (Yammine et al., 2019). Notably, we were able to detect fluorescence quenching in all the p53 family proteins, which indicated a potential binding of LEM3 to p53 ($K_b = 3.7 \times 10^4$ M; $R^2 = 0.98$) (Fig. 4A), TAp63 ($K_b = 6.2 \times 10^4$ M; $R^2 =$

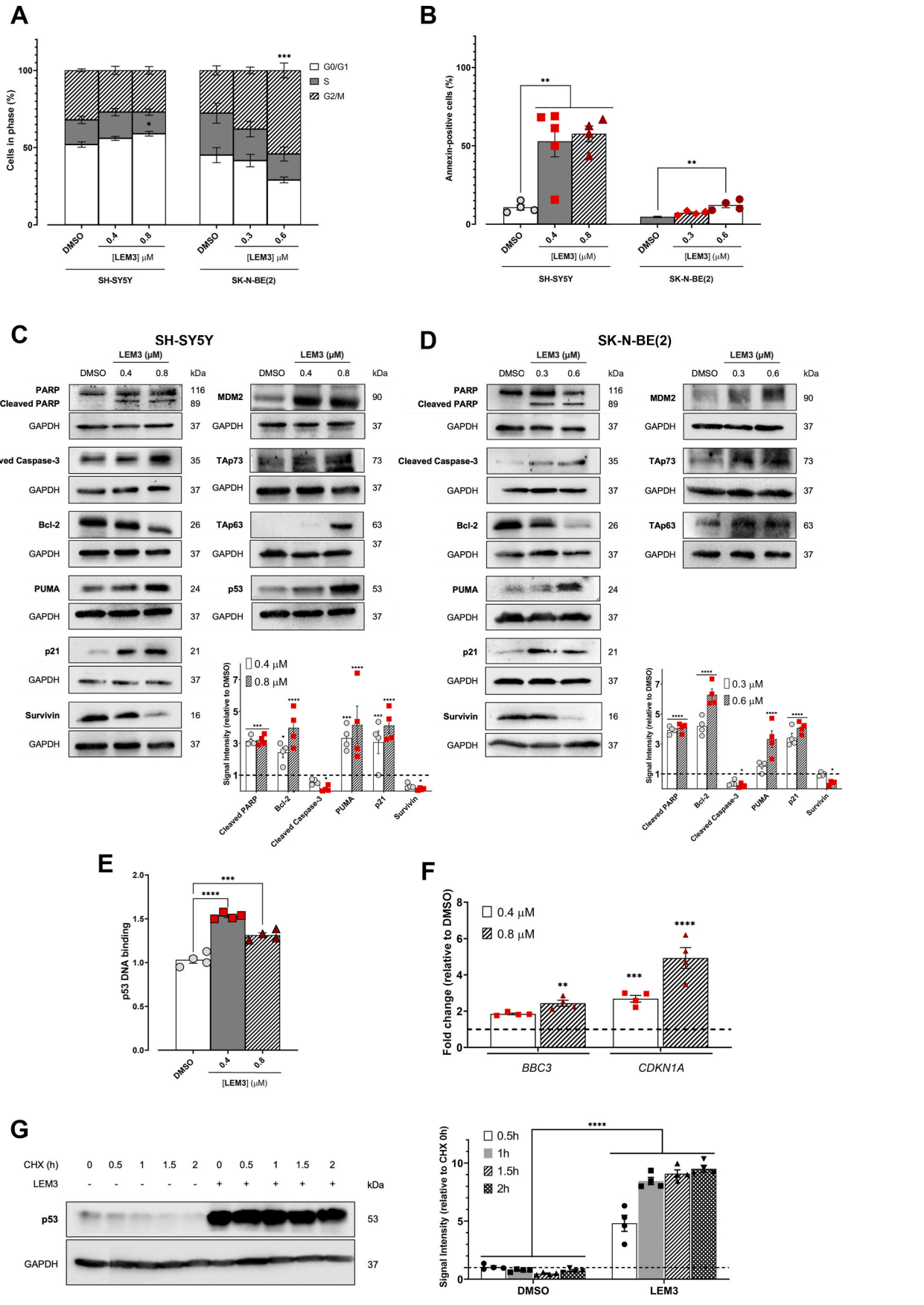

(caption on next page)

Fig. 2. LEM3 activates p53, TAp63 and TAp73, leading to cell cycle arrest and apoptosis. (**A**) Cell cycle analysis in SH-SY5Y and SK-N-BE(2) cells was determined after 24 h of treatment with 0.4 and 0.8 μM of LEM3 and 0.3 and 0.6 μM of LEM3. Data are mean ± SD (n = 4); values are significantly different from DMSO: *p < 0.05, ***p < 0.001, two-way ANOVA with Dunnett's multiple comparison test. (**B**) Apoptosis (Annexin V-positive cells) was evaluated in SH-SY5Y and SK-N-BE(2) cells after 48 h of treatment with 0.4 and 0.8 μM of LEM3. Data are mean ± SD (n = 4); values are significantly different from DMSO: **p < 0.01, one-way ANOVA with Dunnett's multiple comparison test. (**C**, **D**) Protein levels of markers associated with apoptosis and cell cycle (cleaved PARP, cleaved caspase-3, Bcl-2, PUMA, p21 and survivin) and of MDM2, TAp73, TAp63 and p53 in SH-SY5Y (**C**) and SK-N-BE(2) (**D**) cells treated with LEM3 for 48 h. Immunoblots are representative of four independent assays; GAPDH was used as a loading control; quantification of protein expression levels relative to DMSO is shown (set as 1). Data are mean ± SD (n = 4), values are significantly different from DMSO: *p < 0.05, ***p < 0.001, ****p < 0.0001, two-way ANOVA with Dunnett's multiple comparison test. (**E**) DNA binding affinity of wtp53 after 24 h with 0.4 μM (IC_{50}) and 0.8 μM (2 × IC_{50}) of LEM3 in SH-SY5Y cells; the signal obtained with DMSO only was set as 1. Data are mean ± SD (n = 4); values significantly different from DMSO: ***p < 0.001, ****p < 0.0001, one-way ANOVA with Dunnett's multiple comparison test. (**F**) mRNA levels of p53 family transcriptional targets BBC3 and CDKN1A measured by RT-qPCR in SH-SY5Y cells after 16 h with 0.4 and 0.8 μM of LEM3. Fold change is relative to solvent. Data are mean ± SD (n = 4), values are significantly different from DMSO: **p < 0.01, ***p < 0.001, ****p < 0.0001, two-way ANOVA with Dunnett's multiple comparison test. (**G**) p53 protein levels in SH-SY5Y cells treated for 24 h with 0.4 μM of LEM3 or solvent followed by cycloheximide treatment from 0 to 2 h (CHX; 150 μg/mL). Immunoblots are representative of four independent experiments; GAPDH was used as loading control; quantification of protein expression levels relative to DMSO is shown (set as 1). Data are mean ± SD (n = 4), values are significantly different from DMSO: ****p < 0.0001, two-way ANOVA followed by Sidak's test.

0.98) (Fig. 4C) and TAp73 ($K_b = 5.1 \times 10^4$ M; $R^2 = 0.99$) (Fig. 4E).

To further support these findings, LEM3 was subjected to *in silico* docking studies involving the binding of LEM3 to the three proteins of the p53 family. A flexible docking protocol was applied for studying protein-ligand interactions, while accounting for the dynamic nature of the p53 family TA domain.

The TA domain of the p53 family proteins contains a region that can form an α-helix. This helix is crucial for p53 family members to interact with other proteins, including MDM2, which regulate its stability and activity. The TA domain is intrinsically disordered but can adopt structured conformations upon binding to the target (Wells et al., 2008). In all three proteins — p53 (Phe-19), TAp63 (Phe-55), and TAp73 (Phe-15) — a phenylalanine residue is highly conserved and plays a pivotal role in anchoring the protein within the hydrophobic pocket of MDM2. Similarly, a tryptophan residue is conserved across p53 (Trp-23), TAp63 (Trp-59), and TAp73 (Trp-19); this residue is essential for forming strong van der Waals interactions with MDM2, thereby stabilizing the complex. A leucine residue — Leu-26 in p53, Leu-62 in TAp63, and Leu-22 in TAp73 — is also conserved and it contributes to the overall hydrophobic nature of the interaction, reinforcing the binding (Belyi et al., 2010; Ma et al., 2005; Wang et al., 2023). The conservation of key residues (Phe, Trp, and Leu) across p53, TAp63, and TAp73 highlights the evolutionary importance of the interaction with MDM2 (Arrowsmith, 1999; Danilova et al., 2008; Raj and Attardi, 2017).

Key residues for interaction with MDM2 were selected in the binding site (which included Trp23 in p53, Trp59 in TAp63, and Trp19 in TAp73) for flexibility. LEM3 was predicted to bind with the highest affinity to p53 (−3.6 kcal mol^{-1}) through several hydrogen interactions with residues Leu-26 and Glu-28; π-stacking interactions with Trp-23 and halogen bonds with Lys-24 are also formed (Fig. 4B). LEM3 docked to TAp63 with lower affinity (−1.7 kcal mol^{-1}); π-stacking interactions were also established with Trp-59 and Phe-55 (Fig. 4D). LEM3 was predicted to bind to TAp73 with an intermediate affinity (−3.1 kcal mol^{-1}). Several hydrogen interactions are established with residues Ser-20 and Glu-16; π-stacking interactions are established with Phe-15 and Trp-19 (Fig. 4E).

3.6. LEM3 reduces the protein levels of NB-associated biomarkers of poor prognosis, particularly N-Myc

We further found that LEM3 reduced the levels of relevant markers related to NB, including ALK, neuropilin-2, Itch (also known as AIP4), AURKA and Lin-28, in both SH-SY5Y and SK-N-BE(2) cells, after 48 h of treatment (Fig. 5A). ALK amplification is related to poor prognosis (Bellini et al., 2021), while neuropilin-2 is involved in the maintenance of neuronal stemness (Harapin et al., 2015). On the other hand, Itch is known to negatively regulate TAp73 in NB (Meng et al., 2020), while AURKA and Lin-28 are involved in the N-Myc pathways, namely by enhancing N-Myc expression (Jain et al., 2024; Tao et al., 2020).

Notably, LEM3 markedly decreased the levels of N-Myc, both at protein and mRNA levels, in NB cells. In fact, in SH-SY5Y, SK-N-BE(2), KELLY, and LAN-5 cells, LEM3 caused a dose-dependent reduction of N-Myc levels (Fig. 5B; only the lower band, corresponding to the predicted molecular weight of N-Myc, was quantified for densitometric analysis; both bands are shown in the cropped image to preserve the original blot context). Interestingly, in SH-SY5Y cells, the effect of 0.4 μM of LEM3 on N-Myc depletion was more pronounced than that of 10 μM of 13-cis-Retinoic Acid (13cisRA), a well-established inhibitor of N-Myc expression (Nakamura et al., 2003) (Fig. 5B). This was further supported by RT-qPCR data, where 0.1–0.4 μM (IC_{50}) of LEM3 significantly decreased *MYCN* mRNA levels, in SH-SY5Y, SK-N-BE(2), SK-N-AS, and CHP134 cells (Fig. 5C). Of note, SK-N-AS and CHP134 cells are known for their resistance and sensitivity to 13cisRA, respectively (Inamori et al., 2006; Li et al., 2022; Nakamura et al., 2003). As expected, unlike LEM3, 10 μM of 13cisRA did not interfere with *MYCN* transcriptional levels, in SK-N-AS cells (Fig. 5C).

3.7. LEM3 is effective against MYCN-amplified NB cells in a vasculature stiffness model

While NB is primarily a tumor of neural crest origin, its progression and metastatic behavior are tightly linked to the tumor vasculature and its mechanical properties. In high-risk NB, particularly those with aggressive angiogenic profiles, the vasculature often exhibits abnormal structure and function, including increased stiffness, irregular endothelial alignment, and compromised barrier integrity. These features contribute to altered perfusion, hypoxia, and inefficient drug delivery — all hallmarks of poor prognosis (Bao et al., 2022). To explore this dimension, we investigated the efficacy of LEM3 in *MYCN*-amplified NB cells (KELLY) using a stiffness-controlled culture system designed to replicate the mechanical properties of arterial and venous tissues (Zhang and Zhang, 2025). This vascular stiffness model offers a valuable platform to study how mechanical properties of the vascular microenvironment affect NB, known as endothelial interactions. Increased stiffness of the vascular wall, mimicking the remodeling seen in tumor-associated vessels, has been shown to promote endothelial dysfunction, enhanced permeability, and inflammatory adhesion molecule expression. Incorporating vascular stiffness into NB studies therefore offers clinically relevant insight into the biomechanical barriers to effective treatment, particularly in the context of drug delivery, tumor dissemination, and vascular-targeted therapies (Villasante et al., 2024).

To determine the optimal mechanical environment for *MYCN* expression, KELLY cells were cultured on substrates of different stiffness: 4–7 kPa, 100 kPa, and 140 kPa. The KELLY cell line (*MYCN*-amplified, *TP53*-mutant) was selected for this assay as it represents a high-risk NB model, thereby providing a stringent test of compound efficacy. Most importantly, KELLY cells exhibited stable adherence and growth on the

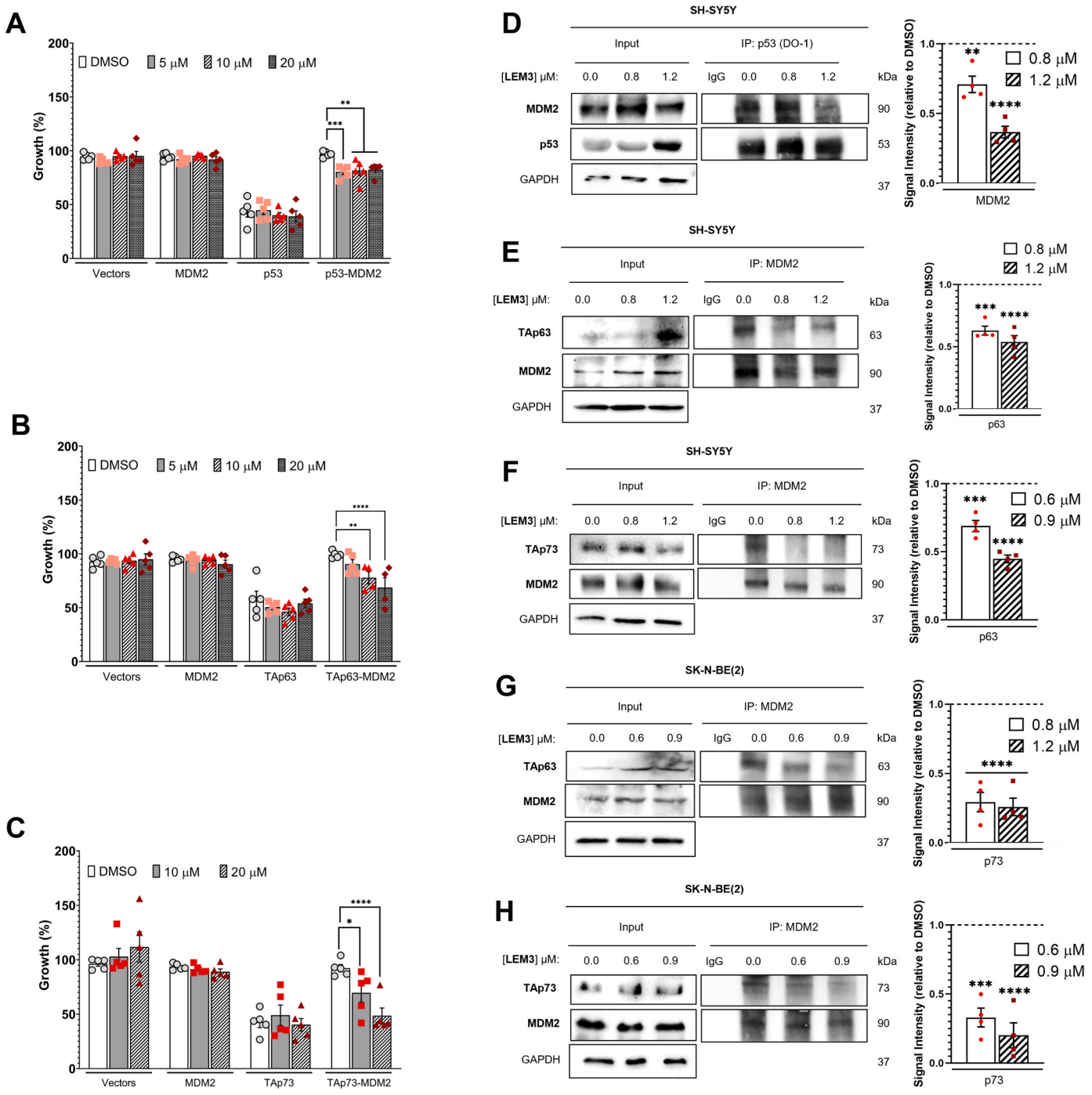

Fig. 3. LEM3 activates p53, TAp63, and TAp73 through disruption of their interaction with MDM2, both in yeast and NB cells. (**A**) Effect of LEM3 on the growth of control yeast (empty vectors), yeast expressing MDM2 or p53 alone, and yeast co-expressing p53 and MDM2, after 40 h of treatment. (**B**) Effect of LEM3 on the growth of control yeast (empty vectors), yeast expressing MDM2 or TAp63 alone, and yeast co-expressing TAp63 and MDM2, after 40 h of treatment. (**C**) Effect of LEM3 on the growth of control yeast (empty vectors), yeast expressing MDM2 or TAp73 alone, and yeast co-expressing TAp73 and MDM2, after 40 h of treatment. In (**A**–**C**), results were plotted setting the growth of untreated control yeast as 100 %. Data are mean ± SD (n = 4); values significantly different from DMSO: *p < 0.05, **p < 0.01, ***p < 0.001, ****p < 0.0001, two-way ANOVA with Dunnett's multiple comparison test. Co-immunoprecipitation (Co-IP) was performed in (**D, E**) SH-SY5Y and (**F, G**) SK-N-BE(2) cells treated with LEM3 for 16 h. Immunoblots are representative of four independent experiments - whole-cell lysate (Input). GAPDH was used as a loading control. Quantification of protein expression levels relative to DMSO is shown (set as 1). Data shown are mean ± SD (n = 4), values are significantly different from DMSO: **p < 0.01, ***p < 0.001, ****p < 0.0001, two-way ANOVA with Dunnett's multiple comparison test.

in vitro vascular stiffness matrices, ensuring assay reproducibility (Chesler et al., 2008; Molenaar et al., 2012). Quantitative PCR revealed that *MYCN* mRNA expression was highest, and significantly upregulated, on the 100 kPa substrate (Fig. 6A). This stiffness falls within the physiological range of arterial tissues, suggesting that it provides a relevant biomechanical context to model aggressive, *MYCN*-driven NB behavior. Based on these findings, the 100 kPa condition was selected for subsequent drug testing.

KELLY cells were then seeded on both plastic and 100 kPa substrates for one week and subsequently treated with DMSO, 1 or 2 μM of LEM3

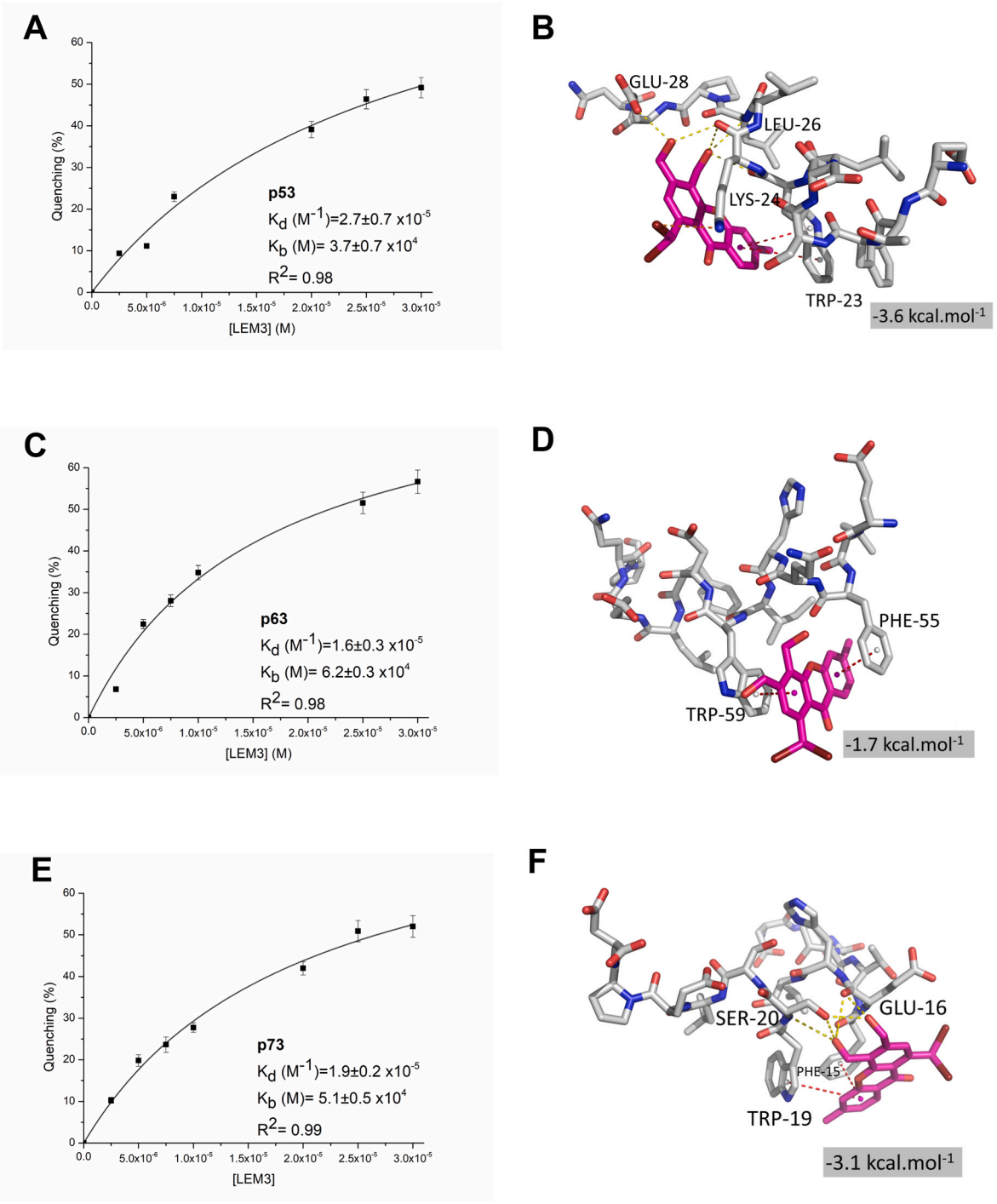

Fig. 4. LEM3 potentially binds to p53, TAp63 and TAp73. Binding of LEM3 to p53 family proteins measured by fluorescence quenching of (**A**) p53, (**C**) TAp63α and (**E**) TAp73α recombinant proteins upon LEM3 titration. The K_d and K_b for the interaction was determined via nonlinear regression using the equation described in Materials and Methods. Detailed view of LEM3 (pink sticks) docked in top scored (**B**) p53, (**D**) TAp63 and (**F**) TAp73 binding sites. Hydrogen, halogen, and π-stacking interactions are represented with yellow, orange, and red broken lines, respectively. Residues involved in those interactions are represented as sticks and labeled.

for 72 h. Cell proliferation analysis showed that LEM3 significantly reduced the growth of NB cells cultured on plastic at both concentrations. However, on the 100 kPa substrate, only the 2 μM dose produced a statistically significant reduction in cell growth (Fig. 6).

To further assess the impact of substrate stiffness on LEM3-induced cytotoxicity, LIVE/DEAD staining was performed at 48 h and 72 h post-treatment (Fig. 6C–H). At both time points, treatment with 1 and 2 μM of LEM3 markedly reduced the number of Calcein-positive (viable) cells in cultures on plastic (Fig. 6D–G). In contrast, for cells grown on 100 kPa substrates, only the 2 μM treatment resulted in a significant decrease in viability (Fig. 6E–H).

Collectively, these results highlight several important conclusions. First, LEM3 demonstrates clear cytotoxic activity against *MYCN*-amplified NB cells, a high-risk clinical subgroup. Second, substrate stiffness modulates this response, suggesting that the physical properties of the tumor microenvironment can influence drug efficacy. Notably, even under vascular-like stiffness conditions (100 kPa), LEM3 retained its anti-tumor effect, reinforcing its potential utility in clinically aggressive

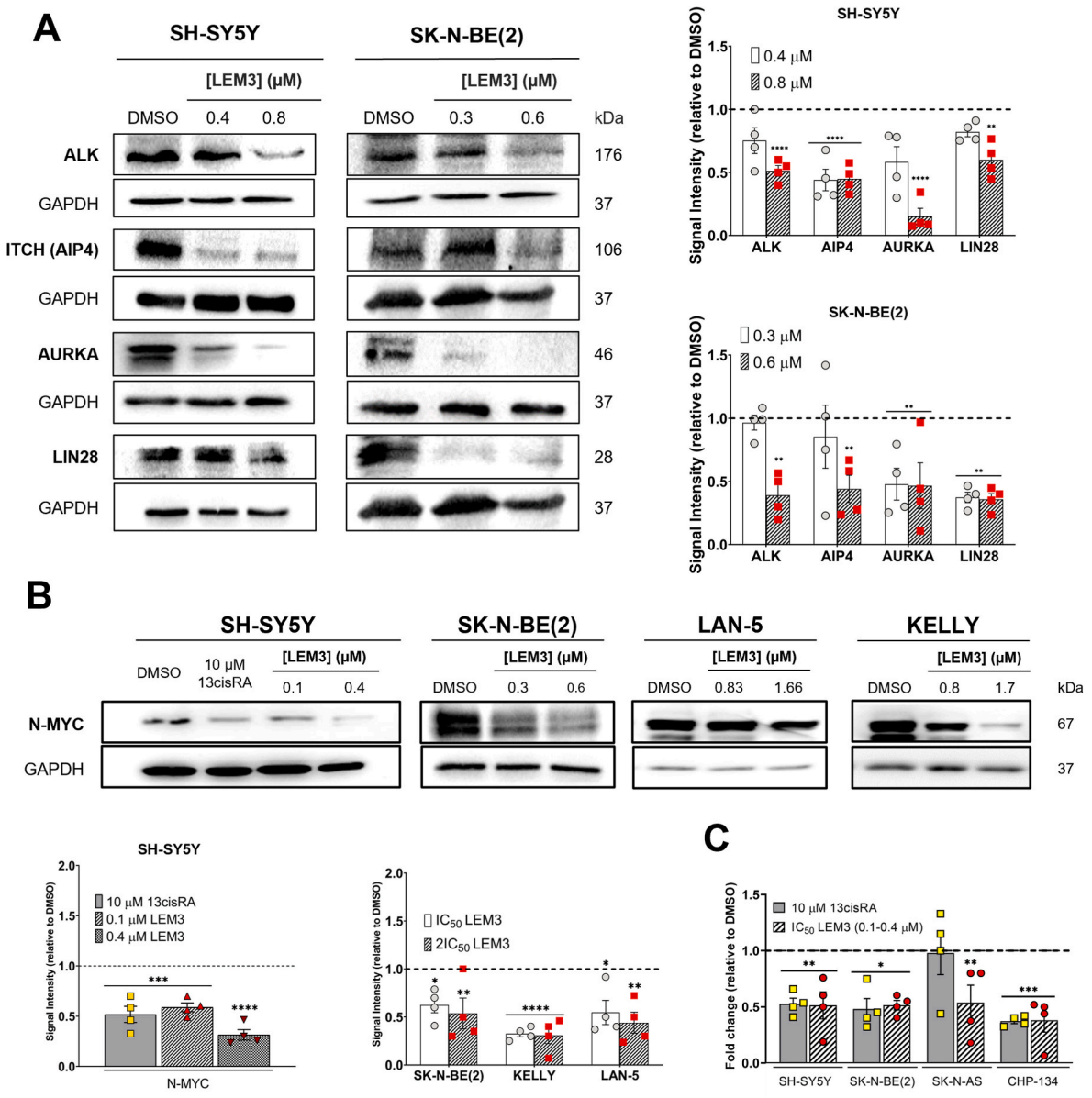

Fig. 5. LEM3 downregulates NB-associated markers related to poor prognosis, with a pronounced impact on N-Myc expression. (**A**) Protein levels of ALK, Neuropilin-2, ITCH, AURKA, and LIN28 in SH-SY5Y and SK-N-BE(2) cells. Immunoblots are representative of four independent experiments, GAPDH was used as a loading control; quantification of protein expression levels relative to DMSO is shown (set as 1). Data shown are mean ± SD (n = 4), values are significantly different from DMSO: **p < 0.01, ****p < 0.0001, two-way ANOVA with Dunnett's multiple comparison test. (**B**) Protein levels of N-Myc in SH-SY5Y, SK-N-BE(2), LAN-5 and KELLY cells. Immunoblots are representative of four independent experiments; 10 μM of 13-cis-Retinoic Acid (13cisRA) was used as a positive control; GAPDH was used as a loading control; quantification of protein expression levels relative to DMSO is shown (set as 1). Data shown are mean ± SD (n = 4), values are significantly different from DMSO: *p < 0.05, **p < 0.01, ***p < 0.001, ****p < 0.0001, two-way ANOVA with Dunnett's multiple comparison test. (**C**) mRNA levels of *MYCN* measured by RT-qPCR after 16 h. Fold of induction is relative to solvent. Data are mean ± SD (n = 4), values are significantly different from DMSO: *p < 0.05, **p < 0.01, ***p < 0.001, two-way ANOVA with Dunnett's multiple comparison test.

NB phenotypes.

3.8. LEM3 reduces NB cell invasion and migration

Given the prominent metastatic behavior of NB and the negative impact this feature has on patient outcomes, we investigated the effect of LEM3 on invasion and migration of SH-SY5Y and SK-N-BE(2) cells. The antimigratory activity of LEM3 was first evaluated by the wound-healing assay. Nevertheless, due to the co-existence of a mixed population of adherent and floating cells in SK-N-BE(2) cultures, we were only able to successfully replicate this assay using the adherent SH-SY5Y cells. For 24 and 48 h, 0.13 and 0.18 μM of LEM3 (concentrations having no significant effect on cell proliferation) reduced wound closure (Fig. 7A and B). Consistently, 0.13 μM of LEM3 also significantly inhibited the migration of SH-SY5Y and SK-N-BE(2) cells through a microporous membrane in the chemotaxis cell migration assay (Fig. 7C). Critically, LEM3 also reduced the ability of these cells to invade through an ECMatrix layer (Fig. 7D).

Accordingly, we also verified that LEM3 inhibited epithelial-to-mesenchymal transition (EMT) markers in SH-SY5Y and SK-N-BE(2) cells (Fig. 7E). Given that EMT dynamics are largely regulated at the post-transcriptional and post-translational levels, our analysis focused

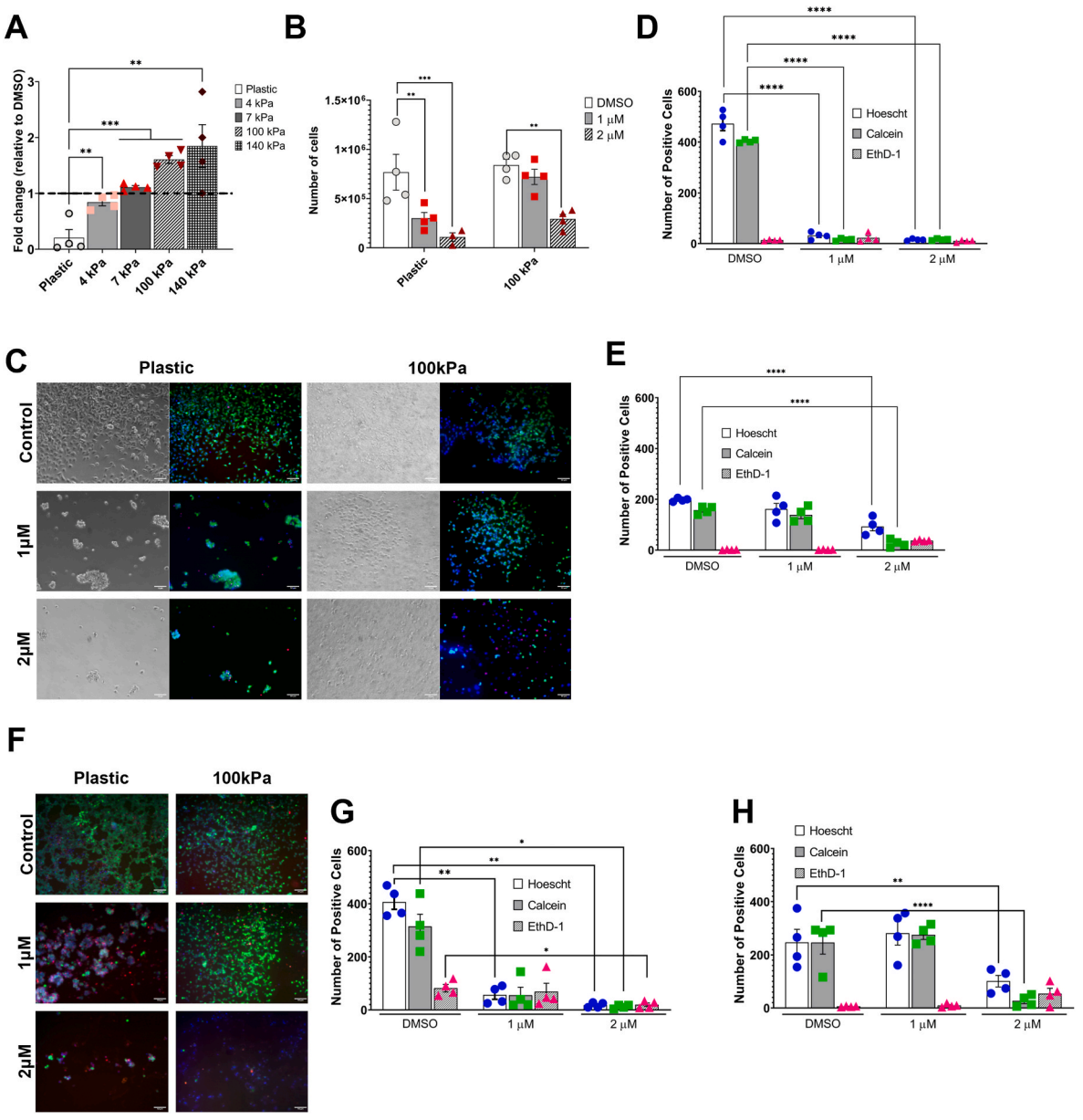

Fig. 6. LEM3 decreases the growth of a *MYCN*-amplified NB cell line in a vasculature-like stiffness model. (A) *MYCN* mRNA expression measured by qRT-PCR in Kelly cells cultured on substrates of varying stiffness (4–7 kPa, 100 kPa, and 140 kPa). Data are mean ± SD (n = 4) values are significantly different from Plastic: **p < 0.01, ***p < 0.001, unpaired *t*-test. **(B)** Cell number in cultures grown on plastic or 100 kPa substrates after 72 h of treatment with DMSO, 1 or 2 μM of LEM3. Data are mean ± SD (n = 4). **p < 0.01, ***p < 0.001, two-way ANOVA followed by Sidak's test. **(C, F)** Representative fluorescence images of Kelly cells stained with Hoechst (nuclei, blue), Calcein-AM (live cells, green), and Ethidium Homodimer-1 (dead cells, red), at 48 h (**C**) and 72 h (**F**) post-treatment. Scale bar: 50 μm. **(D, E, G, H)** Quantification of Calcein-positive (live) cells from images in (**C**, **F**), for plastic (**D**, **G**) and 100 kPa substrates (**E**, **H**) at 48 h and 72 h, respectively. Data are mean ± SD (n = 4), values are significantly different from DMSO: *p < 0.05, **p < 0.01, ****p < 0.0001, two-way ANOVA followed by Tukey's test.

on the protein expression of key EMT markers, which directly reflect phenotypic changes in cell morphology and adhesion. Previous reports have shown that alterations in the abundance and localization of E-cadherin, N-cadherin, and related effectors can occur independently of mRNA levels (Lamouille et al., 2014; Nieto et al., 2016). In fact, LEM3 at 0.4 and 0.8 μM (in SH-SY5Y cells) and 0.3 and 0.6 μM (in SK-N-BE(2) cells) increased E-cadherin while decreasing N-cadherin, β-catenin, Fascin1, SLUG, twist, and N-RAS protein levels. Interestingly, a decrease in the angiogenic factor VEGF was also detected in both NB cell lines (Fig. 7E).

3.9. *LEM3 sensitizes NB cells to standard chemotherapy*

The potential synergistic combination of LEM3 with chemotherapeutic drugs currently used in NB therapy, such as doxorubicin and cisplatin, was assessed by MTT assay, in SH-SY5Y and SK-N-BE (2) cells. One specific concentration of LEM3 (ranging from 0.09 to 0.18 μM; and having no significant effect on NB cell growth) was tested with a range of concentrations of cisplatin (Fig. 8A and B) and doxorubicin (Fig. 8E and F), in SH-SY5Y and SK-N-BE(2) cells. Using the CompuSyn software, a multiple drug-effect analysis was performed for each combination, and the combination index (C.I.) and dose reduction index (D.R.I.) values were calculated. Based on C.I. values, synergistic effects were obtained for most of the tested concentrations (C.I. < 1.0). In particular, for cisplatin, synergistic effects were observed for LEM3 and 2, 4, and 8 μM of cisplatin in SH-SY5Y (Fig. 8A) and SK-N-BE(2) (Fig. 8B) cells. The results also showed that the synergistic effects obtained with these combinations were associated with increased apoptosis (Annexin

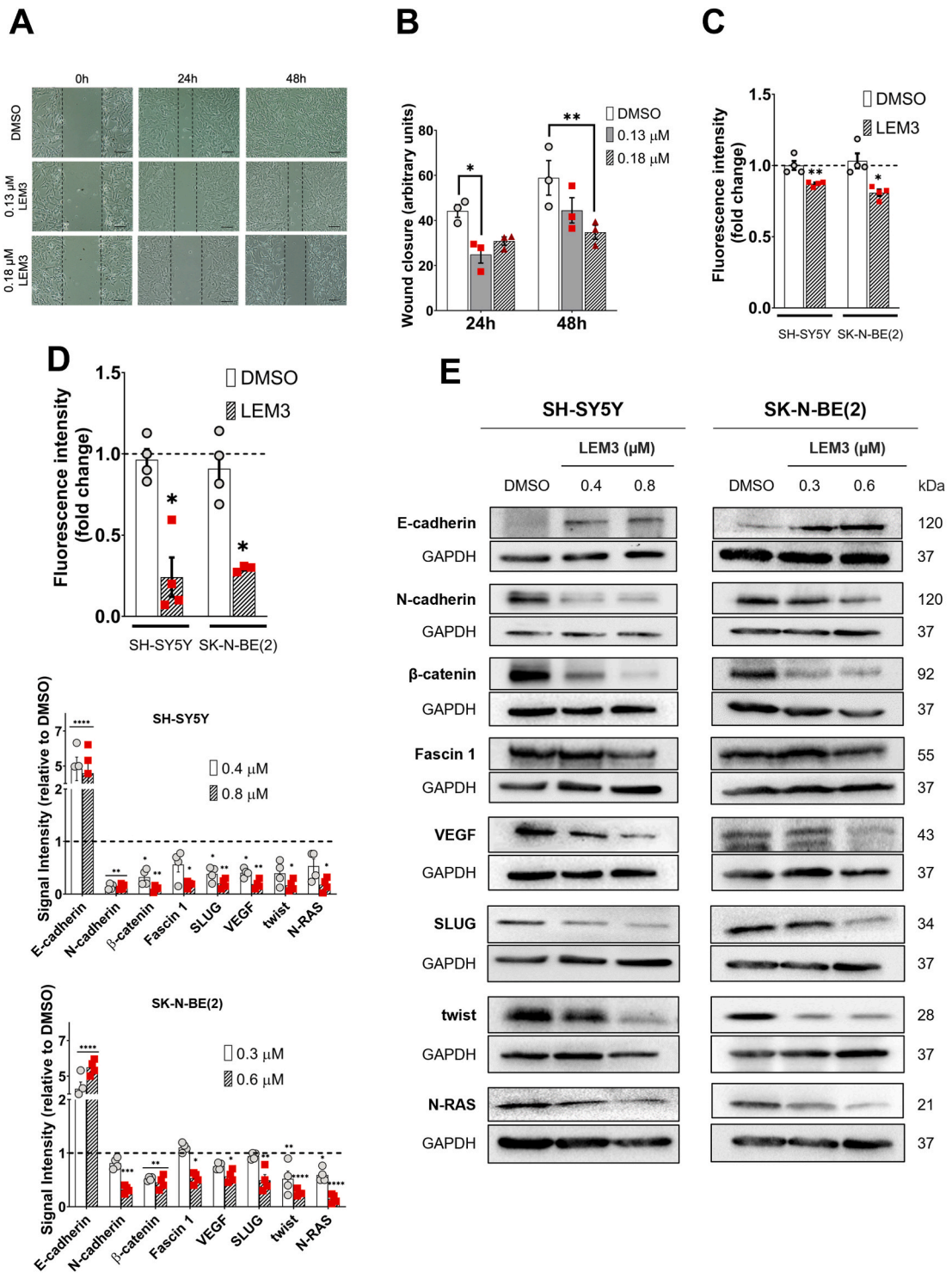

Fig. 7. LEM3 suppresses cell invasion and migration by modulating key regulators of EMT and Angiogenesis. (**A**) SH-SY5Y confluent cells were treated with 0.13 or 0.18 μM of LEM3; cells were observed at 24 and 48 h in the wound-healing assay. Images are representative of four independent experiments; scale bar = 100 μM; magnification = 100×. (**B**) Quantification of wound closure using randomly selected microscopic fields (six fields per sample). Data are mean ± SD (n = 4); values are significantly different from DMSO: *p < 0.05; **p < 0.01, two-way ANOVA followed by Sidak's test. (**C**) Effect of 0.13 μM of LEM3 on migration of SH-SY5Y and SK-N-BE(2) cells after 24 h of treatment. The relative number of migratory cells was determined by analysis of fluorescence signal intensity; values with DMSO were set as 1. Data are mean ± SD, n = 4 (two replicates each); values are significantly different from DMSO: *p < 0.05, Student's *t*-test. (**D**) Effect of 0.13 μM of LEM3 on the invasion of SH-SY5Y and SK-N-BE(2) cells after 24 h of treatment. Cells able to invade through an ECMatrix layer were quantified by fluorescence signal; values with DMSO were set as 1. Data are mean ± SD (n = 4; two replicates each); values are significantly different from DMSO: *p < 0.05, Student's *t*-test. (**E**) Protein expression levels of crucial regulators of EMT and angiogenesis in SH-SY5Y and SK-N-BE(2) cells. Immunoblots are representative of four independent experiments, GAPDH was used as a loading control; quantification of protein expression levels relative to DMSO is shown (set as 1). Data shown are mean ± SD (n = 4), values are significantly different from DMSO: *p < 0.05; **p < 0.01; ***p < 0.001, ****p < 0.0001, two-way ANOVA with Dunnett's multiple comparison test.

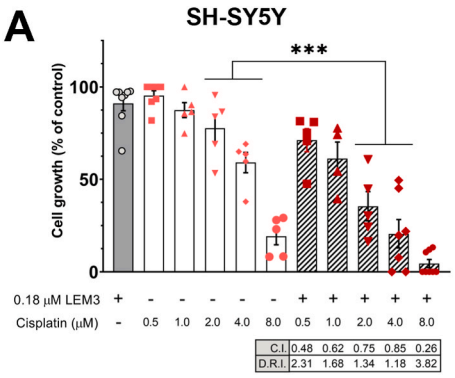

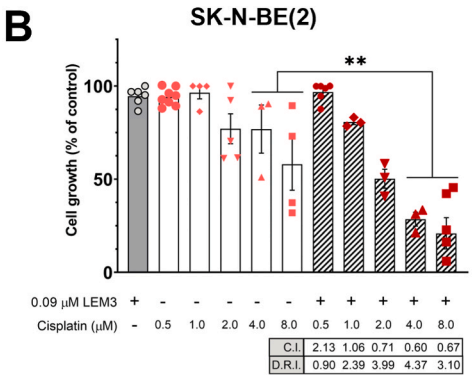

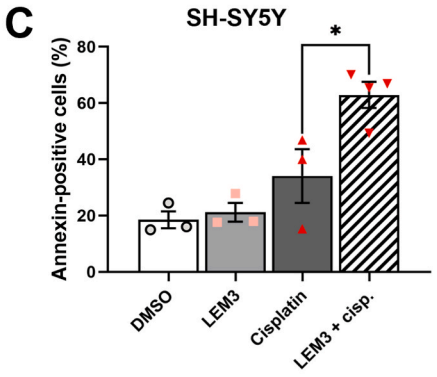

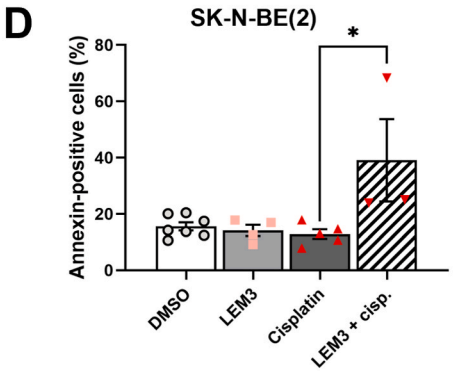

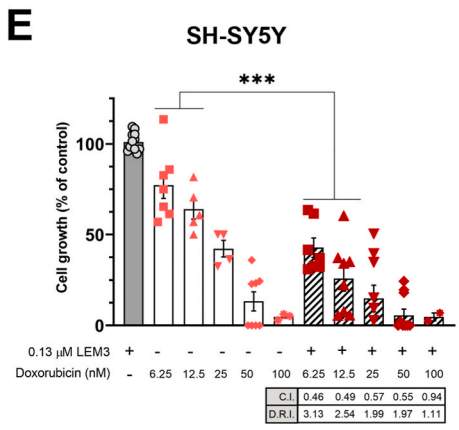

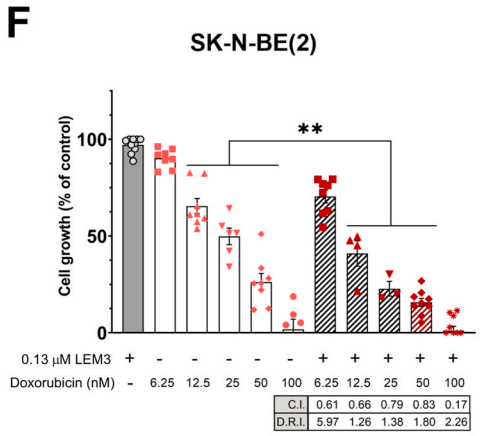

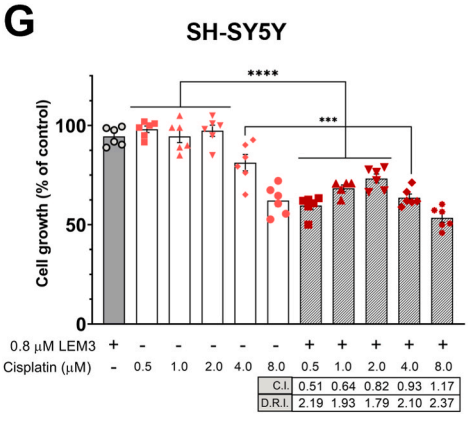

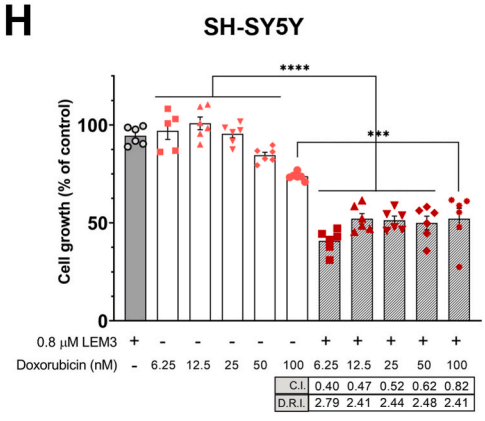

(caption on next page)

Fig. 8. LEM3 sensitizes NB cells to standard chemotherapy. (**A-E**) SH-SY5Y and (**B-F**) SK-N-BE(2) cells were treated with a concentration range of (**A, B**) cisplatin and doxorubicin (**E, F**) alone and in combination with (**A**) 0.18 μM, (**B**) 0.09 μM and (**E, F**) 0.13 μM of LEM3, for 48 h, and the growth was analyzed by MTT assay. Growth with DMSO was set as 100 %. For each combination, the combination index (C.I.) and dose reduction index (D.R.I.) values were obtained. Data are mean ± SD (n = 4; two replicates each); values are significantly different from chemotherapeutic drug alone: $^{**}p < 0.01$, $^{***}p < 0.001$; one-way ANOVA followed by Tukey's test. (**C, D**) Apoptosis (Annexin V-positive cells) was evaluated in (**C**) SH-SY5Y and (**D**) SK-N-BE(2) cells after 48 h of treatment with (**C**) 0.18 μM of LEM3 and 4 μM of cisplatin, (**D**) 0.09 μM of LEM3 and 4 μM of cisplatin. Data are mean ± SD (n = 4); values are significantly different from drug alone: $^{*}p < 0.05$, one-way ANOVA followed by Tukey's test. (**G, H**) SH-SY5Y spheroids were treated with a concentration range of cisplatin (**G**) or doxorubicin (**H**) alone and in combination with 0.8 μM of LEM3 for 48 h, and the growth was analyzed by ATP assay. Cell viability was expressed as a percentage relative to the solvent control. Data were expressed as mean ± SD (n = 4), $^{***}p < 0.001$, $^{****}p < 0.0001$, one-way ANOVA followed by Tukey's test.

V-positive cells), in particular for 0.18 μM of LEM3 and 4 μM of cisplatin in SH-SY5Y cells (Fig. 8C), and for 0.09 μM of LEM3 and 4 μM of cisplatin in SK-N-BE(2) cells (Fig. 8D). It is noteworthy that, for some concentrations of cisplatin, the addition of LEM3 was able to cause a 2- to 4-fold dose reduction to achieve the same level of growth inhibition, in both SH-SY5Y (Fig. 8A) and SK-N-BE(2) (Fig. 8B) cells. Strong synergistic effects were also observed for 0.13 μM of LEM3, in SH-SY5Y cells (Fig. 8E) and SK-N-BE(2) cells (Fig. 8F), at all tested concentrations of doxorubicin. Once again, a 2- to 5-fold reduction of doxorubicin dose was achieved, for some concentrations of this chemotherapeutic agent, in combination with LEM3, in SH-SY5Y (Fig. 8E) and SK-N-BE(2) (Fig. 8F) cells.

These results were further corroborated in a 3D spheroid model of SH-SY5Y cells, in which we evaluated the combination of LEM3 with cisplatin (Fig. 8G) or doxorubicin (Fig. 8H). In particular, spheroids were treated with 0.8 μM of LEM3 alone and in combination with a range of concentrations of these chemotherapeutic agents. As single agents, cisplatin and doxorubicin significantly decreased spheroid viability only at the highest tested concentration. However, in a combination regimen, synergistic effects with a marked reduction in the spheroid growth were observed for 0.5–4 μM of cisplatin (Fig. 8G), and for all tested concentrations of doxorubicin (Fig. 8H). Also, in spheroids of SH-SY5Y cells, LEM3 caused a 2- to 3-fold reduction of cisplatin (Fig. 8G) and doxorubicin (Fig. 8H) doses.

4. Discussion

Xanthones are an important class of oxygen-containing heterocycles (*O*-heterocycles) with several compounds currently being studied in clinical research (Gomes et al., 2016). As a privileged structure, this class of compounds allows for a wide range of substitutions, which can modulate numerous biological responses, like antitumoral effects, making xanthones a promising and intriguing framework for drug development (Resende et al., 2020a). In fact, in our previous work, the xanthone LEM2 also showed promising antiproliferative activity against NB through TAp73 activation (Gomes et al., 2019). However, its poor solubility compromised *in vivo* studies and rendered further studies unfeasible.

In the present study, we report the xanthone derivative LEM3 as an activator of the tumor suppressor proteins p53, TAp63 and TAp73, and with potent antitumor activity by inducing cell cycle arrest and apoptosis. The pronounced growth inhibitory effect of LEM3 was confirmed across a panel of NB cell lines with distinct p53 status and *MYCN* amplification. To investigate the mechanism of action of LEM3 in NB cells, we selected SH-SY5Y (p53 wild-type, *MYCN* non-amplified) and SK-N-BE(2) (p53 mutant, *MYCN*-amplified) cell lines, representing key genetic backgrounds. Given the comparable antiproliferative effects of LEM3 observed in other NB cell lines, including p53-null cells, we hypothesized that similar molecular responses would also occur in these contexts.

The effectiveness of LEM3 against NB was further validated in patient-derived NB cells, including those with *MYCN* amplification. In fact, in these cells, LEM3 demonstrated a potent cytotoxic effect that was even higher than that of the standard chemotherapeutic drug doxorubicin.

LEM3 was shown to activate p53, increasing its protein stability, transcriptional activity and DNA-binding ability. To further explore the mechanism of p53 stabilization, we checked the ability of LEM3 to disrupt the p53 interaction with MDM2. The results showed that LEM3 could inhibit the p53-MDM2 interaction. However, the marked antitumor activity of LEM3 in mutp53 and p53-null NB cells, indicating also a p53-independent activity, prompted us to hypothesize that LEM3 might also activate other members of the p53 family, specifically TAp63 and TAp73, with significant structural and functional similarities with p53 (Bourdon, 2007). Consequently, we also investigated the effect of LEM3 on the interaction between MDM2 and TAp63, as well as TAp73. Notably, LEM3 was also capable of inhibiting the MDM2 interaction with TAp63 and TAp73. In fact, LEM3 was shown to potentially bind to the three p53 family proteins. In addition, LEM3 computational studies revealed the potential binding of LEM3 at the MDM2-binding site within their TA domain.

Given the challenges of targeting p53 directly, most efforts to inhibit the p53-MDM2 interaction have focused on targeting MDM2. Several small-molecule inhibitors of the p53-MDM2 interaction have been developed, including nutlins, a class of small molecules that bind to the hydrophobic pocket of MDM2, displacing p53 (Resende et al., 2020a). These inhibitors are generally very effective because they exploit the well-defined structure of the MDM2 binding pocket (Bourdon, 2007). However, if a small molecule binds to the p53 TA domain at the interface where MDM2 would normally interact, it could block MDM2 binding in one of two ways: direct steric hindrance (the small molecule physically occupies the binding site, preventing MDM2 from accessing p53) or conformational changes (the small molecule induces a conformational change in p53 that disrupts the ability of MDM2 to recognize and bind to p53) (Zacharioudakis and Gavathiotis, 2022). This would stabilize p53 and prevent its degradation, leading to increased p53 levels and activation of its downstream tumor suppressor functions. However, it is important to consider that MDM2 binds to p53 with high affinity. For a small molecule to effectively compete with MDM2, it must also bind with similarly high affinity, which is a significant challenge. Moreover, while the MDM2 binding pocket is well-defined, with a structured cavity, making it a more tractable target for small-molecule inhibitors, the p53 TA domain α-helix structure makes it challenging to design small molecules that can specifically and tightly bind to this region (Chi et al., 2005; Raj and Attardi, 2017).

Collectively, these results indicated a promising therapeutic potential of LEM3 for distinct genetic profiles of NB, particularly regarding p53 status, through activation of p53 family-related pathways. Furthermore, LEM3 has an iLogP value of 2.93, which is below the threshold of 5, indicating favorable lipophilicity. It has two hydrogen bond donors and four hydrogen bond acceptors, and its molecular weight is under 500. These properties align with Lipinski's Rule of Five, suggesting that LEM3 is likely to exhibit good oral bioavailability. Additionally, predictions indicate that LEM3 may demonstrate high gastrointestinal absorption and the ability to penetrate the blood-brain barrier (BBB).

About 20–25 % of NB tumors have *MYCN* amplification, which leads to increased expression of the N-Myc protein. This overexpression is a hallmark of high-risk and aggressive NB (Schwab et al., 1984). In addition to interfering with the levels of several NB-associated markers, reducing ALK, Itch, AURKA, PHOX2B, LEM3 markedly downregulated N-Myc, both at protein and mRNA levels. In fact, LEM3 demonstrated a

reduction in N-Myc levels comparable to that of 13cisRA, a well-known treatment for NB (Broso et al., 2023), at a 100-fold lower dose and in a 13cisRA-resistant NB cell line. The observed reduction in N-Myc levels may be linked to the upregulation of TAp73, which has been shown to downregulate N-Myc by destabilizing *MYCN* mRNA (Horvilleur et al., 2008). Another potential mechanism involving p53 is its indirect role in promoting N-Myc degradation through the downregulation of AURKA. AURKA stabilizes N-Myc by preventing its degradation via the FBXW7 ubiquitin-proteasome pathway (Almeida et al., 2022). As LEM3 induces the upregulation and stabilization of p53, while reducing AURKA levels, N-Myc becomes increasingly vulnerable to proteasomal degradation. This is because the reduction of AURKA impairs its protective function against FBXW7-mediated ubiquitination of N-Myc. In fact, several strategies targeting N-Myc have emerged, including the use of AURKA inhibitors such as alisertib, which has been shown to promote N-Myc degradation (Almeida et al., 2022; Liu et al., 2021).

NB is characterized by its high vascularization, which significantly impacts tumor growth, survival, and metastasis. Numerous studies have emphasized the importance of the tumor microenvironment in facilitating vascular development *in vitro* (Xue et al., 2017). Notably, factors such as substrate stiffness have been identified as particularly influential in promoting vascular formation within these tumors (Villasante et al., 2024). To investigate the effects of LEM3 under defined mechanical conditions, we utilized a previously established model that mimics the stiffness of well-characterized vascular tissues, such as arteries (50–150 kPa) and veins (3–50 kPa) (Gordon et al., 2020; Villasante et al., 2024). We focused on an adrenergic, *MYCN*-amplified cell line, as it is well-documented that *MYCN* amplification contributes to tumor vascularization and increased malignancy (Blavier et al., 2020). Our findings indicated that a substrate stiffness of 100 kPa produced the most favorable conditions for our experiments. Under these conditions, the *MYCN*-amplified cells exhibited optimal levels of N-Myc overexpression, enhancing the likelihood of their transdifferentiation, which is a key mechanism facilitating tumor vascularization (Villasante et al., 2024). Interestingly, the stiffness of collagenous bone, a common site for NB metastasis, is approximately 100 kPa (Murphy et al., 2013). Consistent with our findings on cell proliferation, we observed a significant reduction in cell growth at 1 and 2 μM of LEM3 in cells cultured on plastic substrates. Although cells seeded on the 100 kPa substrate showed a slightly higher resistance, a pronounced inhibitory effect remained evident at 2 μM of LEM3. Interestingly, the study also emphasized the role of the tumor microenvironment, specifically, the stiffness of the substrate, on tumor cell behavior. The observation that the 100 kPa substrate (likely mimicking the physical properties of artery and vein tissues) supports higher *MYCN* overexpression and influences the response to LEM3 indicates that the mechanical properties of the tumor microenvironment play a significant role in tumor biology and treatment response. Most importantly, the results highlight the efficacy of LEM3 against *MYCN*-amplified NB cells within a vascular stiffness context, suggesting that it may hold potential as a therapeutic agent specifically targeting a high-risk group of NB patients. Given that NB often exhibits mechanisms of chemoresistance linked to interactions with the tumor microenvironment (including vascularization and stiffness), these findings may provide insights into overcoming such resistance. Understanding how LEM3 works in various environments possessing different stiffness can guide future therapeutic approaches and facilitate the development of combination therapies that consider both drug action and mechanical properties.

In many patients with stage III and IV NB, relapse typically occurs shortly after chemotherapy and is associated with aggressive tumor behavior, chemotherapy resistance, and organ metastasis (Bhoopathi et al., 2019). Addressing and mitigating metastasis remains a significant clinical challenge (Bhoopathi et al., 2019). Cell invasion is influenced by both extracellular and intracellular factors, requiring dynamic interactions between various cell surface receptors and the extracellular matrix (ECM) (Kamińska et al., 2015). p53 and TAp73 play a key role in regulating several critical components of classical metastasis pathways (Powell et al., 2014). Considering this, we examined the effect of LEM3 on EMT and found that it exhibits potent anti-invasive and anti-migratory properties in NB cells. We evaluated the expression levels of relevant markers associated with EMT inhibition, in NB cells treated with LEM3, and observed an increase in E-cadherin expression alongside with a decrease in N-cadherin, β-catenin, Slug, and Twist levels. The regulation of β-catenin is particularly noteworthy, as components of the WNT/β-catenin signaling pathway have been implicated in NB proliferation. Specifically, in *MYCN* non-amplified cell lines, enhanced WNT/β-catenin signaling has been linked to increased *MYCN* expression levels (Wang et al., 2018). Conversely, silencing *MYCN* expression in *MYCN*-amplified NB cell lines led to reduced viability, increased apoptosis, and ultimately inhibited WNT/β-catenin signaling (Wang et al., 2018). Therefore, the observed reduction in β-catenin levels may correlate with decreased N-Myc expression. Moreover, LEM3 treatment resulted in decreased levels of the angiogenesis-inducing factor VEGF, as well as reduced N-RAS levels, which are considered markers of poor prognosis in NB. N-RAS is frequently mutated in high-risk and relapsed NB cases and is associated with the activation of the RAS-MAPK pathway, which promotes cell survival, proliferation, migration, and invasion (Lin et al., 2022; Mlakar et al., 2021; Pucci et al., 2024). Several of the EMT-related proteins analyzed in this study are known to be regulated by N-Myc, either directly or through downstream transcriptional networks. N-Myc can repress E-cadherin expression, while promoting N-cadherin and Fascin-1, thereby enhancing cell motility and invasiveness (Anderson et al., 2016; Iraci et al., 2011). In addition, N-Myc has been reported to upregulate VEGF, a key angiogenic factor (Hatzi et al., 2002), and to cooperate with β-catenin and RAS signaling pathways to promote tumor progression (Bachireddy et al., 2005; Wang et al., 2018). These findings collectively support a model in which LEM3-mediated downregulation of N-Myc may contribute to the observed modulation of EMT markers and reduced malignancy.

One of the primary causes of therapeutic failure in NB patients is multidrug resistance, where tumor cells become insensitive to various drugs (Zhou et al., 2023). To investigate the potential induction of drug resistance by LEM3, we subjected NB cells to multiple rounds of treatment, gradually increasing the concentration at each round. The absence of changes in the dose of LEM3 indicated that resistance was not induced under the experimental conditions used. However, further studies with longer treatment times will be necessary to confirm these findings.

To evaluate the ability of LEM3 to enhance the antitumor effect of commonly used chemotherapeutic agents in high-risk NB treatment (Ganeshan and Schor, 2011), we tested its combination with cisplatin and doxorubicin, in 2D and 3D cultures. LEM3 exhibited synergistic effects with the two drugs. Consistent with the importance of a functional p53 pathway for the efficacy of many chemotherapies, the calculated dose reduction index showed that LEM3 significantly reduced the effective dose required for each chemotherapeutic agent. Interestingly, both doxorubicin and cisplatin promote the proteasomal degradation of ΔNp73 (Barbieri et al., 2006; Matthay et al., 1999), which is commonly overexpressed in NB and linked to poor prognosis, primarily due to its dominant-negative effect on TAp73 transcriptional activity (Cinatl et al., 2014; Nikolaev et al., 2003). However, these treatments are associated with significant toxic side effects and frequent relapse after remission (Pinto et al., 2015). Sensitizing NB cells to these chemotherapies is a promising therapeutic strategy, as it can reduce NB resistance while minimizing the toxicity caused by high doses of these drugs.

Despite the promising pharmacological properties of LEM3, the compound demonstrated an unfavorable toxicological profile *in vivo*. Specifically, for the dose of 10 mg/kg, the presence of peritonitis was visible in the sacrificed animals (nude mice; none of the 5 animals tested died). As such, we were unable to test the antitumor effect in mice at higher doses of LEM3 (data not shown). While this limitation constrains the use of LEM3 as a standalone therapy, its pharmacological properties

may be advantageous when combined with other chemotherapeutic agents at lower doses. Furthermore, LEM3 has the potential to serve as a valuable starting point for hit-to-lead optimization, possibly leading to new derivatives with safer profiles. This drug development approach could generate new drug candidates with relevant clinical applications for treating *MYCN*-amplified NB. In addition to these prospects, LEM3 shows considerable promise as a valuable tool for functional and pharmacological studies of p53 family proteins, namely in NB.

CRediT authorship contribution statement

Conceptualization, J.A. and L.S.; Formal analysis, all authors; Funding acquisition, A.V., J. Š., P.O., S.R., A.H.P.L., B.C., A.I., E.S. and L. S.; Investigation, all authors; Methodology, J.A., D.I.S.P.R., R.S. A.P., A. V., C.M., V.Z., F.B., A.V., P.O., C.N., and E.M.; Project administration, L. S., Resources, A.V., J. Š., P.O., S.R., A.H.P.L., B.C., A.I., J.S., E.S. and L.S.; Validation, A.V., J. Š, P.O., S.R., A.H.P.L., A.I., J.S., E.S. and L.S.; Writing – original draft, J.A. and L.S.; writing—review and editing, all authors. All authors have read and agreed to the published version of the manuscript.

Declaration of competing interest

The authors declare that they have no known competing financial interests or personal relationships that could have appeared to influence the work reported in this paper.

Acknowledgments

This work received financial support from the PT national funds (FCT/MECI, Fundação para a Ciência e Tecnologia and Ministério da Educação, Ciência e Inovação) through the projects UID/50006 (Laboratório Associado para a Química Verde - Tecnologias e Processos Limpos), 2024.13556.PEX, LA/P/0008/2020 DOI 10.54499/LA/P/0008/2020, UIDP/50006/2020 DOI 10.54499/UIDP/50006/2020, UIDB/50006/2020 DOI 10.54499/UIDB/50006/2020, UIDB/04033/2020 DOI: 10.54499/UIDB/04033/2020 (CITAB), LA/P/0126/2020 DOI: 10.54499/LA/P/0126/2020 (INOV4AGRO), UIDB/50026/2020 DOI 10.54499/UIDB/50026/2020, UIDP/50026/2020 DOI 10.54499/UIDP/50026/2020, and LA/P/0050/2020 DOI 10.54499/LA/P/0050/2020. We also thank FCT for the financial support through the fellowship 2020.05026.BD (Joana Almeida) and through the individual researcher contract (2022.00379.CEECIND) (Diana Resende). Jan Škoda is supported by the project National Institute for Cancer Research (Programme EXCELES, ID Project No. LX22NPO5102)—Funded by the European Union—Next Generation EU. The IBEC Group is supported by Department of Research and Universities of the Generalitat de Catalunya (2021 SGR 01545). CERCA Programme/Generalitat de Catalunya. Networking Biomedical Research Center (CIBER) of Spain. CIBER is an initiative funded by the VI National R&D&i Plan 2008–2011, Iniciativa Ingenio 2010, Consolider Program, CIBER Actions and the Instituto de Salud Carlos III (RD16/0006/0012), with the support of the European Regional Development Fund (ERDF). Aranzazu Villasante is supported by the Scientific Foundation of the Spanish Association Against Cancer (INVES234968VILL). Catherine Murphy is supported by Grant CNS2023-143930 by MCIN/AEI/10.13039/501100011033 and by "European Union NextGenerationEU/PRTR". Veronica Zingales is supported by Generalitat Valenciana (APOSTD/CIAPOS2021). Eduarda P. Martins, Bruno M. Costa and Joana M. Ferreiras are supported by UID/06304/2023 Project NORTE2030-FEDER-02705300, supported by Norte Portugal Regional Operational Programme (NORTE 2030), under the PORTUGAL 2030 Partnership Agreement, through the European Regional Development Fund (ERDF). We thank Petr Chlapek for part of the proliferation results presented on Fig. 1B.

Appendix A. Supplementary data

Supplementary data to this article can be found online at https://doi.org/10.1016/j.ejphar.2025.178295.

Data availability

Data will be made available on request.

References

Agarwal, S., Milazzo, G., Rajapakshe, K., Bernardi, R., Chen, Z., Barberi, E., Koster, J., Perini, G., Coarfa, C., Shohet, J.M., Agarwal, S., Milazzo, G., Rajapakshe, K., Bernardi, R., Chen, Z., Barberi, E., Koster, J., Perini, G., Coarfa, C., Shohet, J.M., 2018. MYCN acts as a direct co-regulator of p53 in MYCN amplified neuroblastoma. Oncotarget 9, 20323–20338. https://doi.org/10.18632/ONCOTARGET.24859.

Almeida, J., Mota, I., Skoda, J., Sousa, E., Cidade, H., Saraiva, L., 2022. Deciphering the role of p53 and TAp73 in Neuroblastoma: from pathogenesis to treatment. Cancers 14. https://doi.org/10.3390/CANCERS14246212. Page 6212 14, 6212.

Anderson, S., Poudel, K.R., Roh-Johnson, M., Brabletz, T., Yu, M., Borenstein-Auerbach, N., Grady, W.N., Bai, J., Moens, C.B., Eisenman, R.N., Conacci-Sorrell, M., 2016. MYC-nick promotes cell migration by inducing fascin expression and Cdc42 activation. Proc. Natl. Acad. Sci. U. S. A. 113, E5481–E5490. https://doi.org/10.1073/PNAS.1610994113.

Armstrong, S.R., Wu, H., Wang, B., Abuetabh, Y., Sergi, C., Leng, R.P., 2016. The regulation of tumor suppressor p63 by the ubiquitin-proteasome System. Int. J. Mol. Sci. 17. https://doi.org/10.3390/IJMS17122041.

Arrowsmith, C.H., 1999. Structure and function in the p53 family. Cell Death Differ. 6, 1169–1173. https://doi.org/10.1038/SJ.CDD.4400619.

Bachireddy, P., Bendapudi, P.K., Felsher, D.W., 2005. Getting at MYC through RAS. Clin. Cancer Res. 11, 4278–4281. https://doi.org/10.1158/1078-0432.CCR-05-0534.

Bálint, E., Bates, S., Vousden, K.H., 1999. Mdm2 binds p73 alpha without targeting degradation. Oncogene 18, 3923–3929. https://doi.org/10.1038/SJ.ONC.1202781.

Bao, M., Chen, Y., Liu, J.T., Bao, H., Wang, W. Bin, Qi, Y.X., Lv, F., 2022. Extracellular matrix stiffness controls VEGF165 secretion and neuroblastoma angiogenesis via the YAP/RUNX2/SRSF1 axis. Angiogenesis 25, 71–86. https://doi.org/10.1007/S10456-021-09804-7.

Barbieri, E., Mehta, P., Chen, Z., Zhang, L., Slack, A., Berg, S., Shohet, J.M., 2006. MDM2 inhibition sensitizes neuroblastoma to chemotherapy-induced apoptotic cell death. Mol. Cancer Therapeut. 5, 2358–2365. https://doi.org/10.1158/1535-7163.MCT-06-0305.

Bellini, A., Potschger, U., Bernard, V., Lapouble, E., Baulande, S., Ambros, P.F., Auger, N., Beiske, K., Bernkopf, M., Betts, D.R., Bhalshankar, J., Bown, N., De Preter, K., Clement, N., Combaret, V., De Mora, J.F., George, S.L., Jimenez, I., Jeison, M., Marques, B., Martinsson, T., Mazzocco, K., Morini, M., Muhlethaler-Mottet, A., Noguera, R., Pierron, G., Rossing, M., Taschner-Mandl, S., Van Roy, N., Vicha, A., Chesler, L., Balwierz, W., Castel, V., Elliott, M., Kogner, P., Laureys, G., Luksch, R., Malis, J., Popovic-Beck, M., Ash, S., Delattre, O., Valteau-Couanet, D., Tweddle, D.A., Ladenstein, R., Schleiermacher, G., 2021. Frequency and prognostic impact of alk amplifications and mutations in the european neuroblastoma study group (siopen) high-risk neuroblastoma trial (Hr-nbl1). J. Clin. Oncol. 39, 3377–3390. https://doi.org/10.1200/JCO.21.00086.

Belyi, V.A., Ak, P., Markert, E., Wang, H., Hu, W., Puzio-Kuter, A., Levine, A.J., 2010. The origins and evolution of the p53 family of genes. Cold Spring Harbor Perspect. Biol. 2, a001198. https://doi.org/10.1101/CSHPERSPECT.A001198.

Bhoopathi, P., Pradhan, A.K., Bacolod, M.D., Emdad, L., Sarkar, D., Das, S.K., Fisher, P.B., 2019. Regulation of neuroblastoma migration, invasion, and in vivo metastasis by genetic and pharmacological manipulation of MDA-9/Syntenin. Oncogene 38 (41), 6781–6793. https://doi.org/10.1038/s41388-019-0920-5.

Blavier, L., Yang, R.M., Declerck, Y.A., 2020. The Tumor microenvironment in Neuroblastoma: new players, new mechanisms of interaction and new perspectives. Cancers 12. https://doi.org/10.3390/CANCERS12102912.

Bourdon, J.-C., 2007. p53 family isoforms. Curr. Pharm. Biotechnol. 8, 332–336. https://doi.org/10.2174/138920107783018444.

Brodeur, G.M., Seeger, R.C., Schwab, M., Varmus, H.E., Michael Bishop, J., 1984. Amplification of N-myc in untreated human Neuroblastomas correlates with advanced disease stage. Science 224, 1121–1124. https://doi.org/10.1126/SCIENCE.6719137.

Broso, F., Gatto, P., Sidarovich, V., Ambrosini, C., De Sanctis, V., Bertorelli, R., Zaccheroni, E., Ricci, B., Destefanis, E., Longhi, S., Sebastiani, E., Tebaldi, T., Adami, V., Quattrone, A., 2023. Alpha-1 adrenergic antagonists sensitize neuroblastoma to therapeutic differentiation. Cancer Res. 83, 2733–2749. https://doi.org/10.1158/0008-5472.CAN-22-1913.

Carr, J., Bell, E., Pearson, A.D.J., Kees, U.R., Beris, H., Lunec, J., Tweddle, D.A., 2006. Increased Frequency of Aberrations in the p53/MDM2/p14ARF Pathway in Neuroblastoma Cell Lines Established at Relapse. Cancer Res. 66, 2138–2145. https://doi.org/10.1158/0008-5472.CAN-05-2623.

Carr-Wilkinson, J., O'Toole, K., Wood, K.M., Challen, C.C., Baker, A.G., Board, J.R., Evans, L., Cole, M., Cheung, N.K.V., Boos, J., Köhler, G., Leuschner, I., Pearson, A.D. J., Lunec, J., Tweddle, D.A., 2010. High frequency of p53/MDM2/p14ARF pathway abnormalities in relapsed neuroblastoma. Clin. Cancer Res. 16, 1108–1118. https://doi.org/10.1158/1078-0432.CCR-09-1865.

Chen, J., Guan, Z., 2022. Function of oncogene mycn in adult neurogenesis and oligodendrogenesis. Mol. Neurobiol. 59, 77–92. https://doi.org/10.1007/s12035-021-02584-7.
Chesler, L., Goldenberg, D.D., Collins, R., Grimmer, M., Kim, G.E., Tihan, T., Nguyen, K., Yakovenko, S., Matthay, K.K., Weiss, W.A., 2008. Chemotherapy-Induced apoptosis in a transgenic model of neuroblastoma proceeds through p53 induction. Neoplasia 10. https://doi.org/10.1593/NEO.08778, 1268-IN34.
Cheung, N.-K.V., Kushner, B.H., LaQuaglia, M., Kramer, K., Gollamudi, S., Heller, G., Gerald, W., Yeh, S., Finn, R., Larson, S.M., Wuest, D., Byrnes, M., Dantis, E., Mora, J., Cheung, I.Y., Rosenfield, N., Abramson, S., O'Reilly, R.J., 2001. N7: a novel multi-modality therapy of high risk neuroblastoma (NB) in children diagnosed over 1 year of age. Med. Pediatr. Oncol. 36, 227–230. https://doi.org/10.1002/1096-911X(20010101)36:1<227::AID-MPO1055>3.0.CO;2-U.
Chi, S.W., Lee, S.H., Kim, D.H., Ahn, M.J., Kim, J.S., Woo, J.Y., Torizawa, T., Kainosho, M., Han, K.H., 2005. Structural details on mdm2-p53 interaction. J. Biol. Chem. 280, 38795–38802. https://doi.org/10.1074/jbc.M508578200.
Chou, T.C., Talalay, P., 1984. Quantitative analysis of dose-effect relationships: the combined effects of multiple drugs or enzyme inhibitors. Adv. Enzym. Regul. 22, 27–55. https://doi.org/10.1016/0065-2571(84)90007-4.
Cinatl, J., Speidel, D., Hardcastle, I., Michaelis, M., 2014. Resistance acquisition to MDM2 inhibitors. Biochem. Soc. Trans. 42, 752–757. https://doi.org/10.1042/BST20140035.
Corvi, R., Savelyeva, L., Breit, S., Wenzel, A., Handgretinger, R., Barak, J., Oren, M., Amler, L., Schwab, M., 1995. Non-syntenic amplification of MDM2 and MYCN in human neuroblastoma. Oncogene 10, 1081–1086.
Danilova, N., Sakamoto, K.M., Lin, S., 2008. p53 family in development. Mech. Dev. 125, 919–931. https://doi.org/10.1016/J.MOD.2008.09.003.
Dobbelstein, M., Wienzek, S., König, C., Roth, J., 1999. Inactivation of the p53-homologue p73 by the mdm2-oncoprotein. Oncogene 18 (12), 2101–2106. https://doi.org/10.1038/sj.onc.1202512.
Fernandes, C., Palmeira, A., Ramos, I.I., Carneiro, C., Afonso, C., Tiritan, M.E., Cidade, H., Pinto, P.C.A.G., Saraiva, M.L.M.F.S., Reis, S., Pinto, M.M.M., 2017. Chiral derivatives of xanthones: investigation of the effect of enantioselectivity on inhibition of cyclooxygenases (COX-1 and COX-2) and binding interaction with human serum albumin. Pharmaceuticals 10. https://doi.org/10.3390/PH10020050. Page 50 10, 50.
Finklestein, J.Z., Gilchrist, G.S., 2010. Recent advances in Neuroblastoma. Calif. Med. 116, 116–127. https://doi.org/10.1056/NEJMRA0804577.
Gamble, L.D., Kees, U.R., Tweddle, D.A., Lunec, J., 2011. MYCN sensitizes neuroblastoma to the MDM2-p53 antagonists Nutlin-3 and MI-63. Oncogene 31 (6), 752–763. https://doi.org/10.1038/onc.2011.270.
Ganeshan, V.R., Schor, N.F., 2011. Pharmacological management of high-risk neuroblastoma in children. Paediatr Drugs 13, 245. https://doi.org/10.2165/11591630-000000000-00000.
Gomes, A.S., Brandão, P., Fernandes, C.S.G., Silva, M.r.p.c. da, Sousa, M.e. da s.p. de, Pinto, M.M. de M., 2016. Drug-like properties and ADME of xanthone derivatives: the antechamber of clinical trials. Curr. Med. Chem. 23, 3654–3686. https://doi.org/10.2174/0929867323666160425113058.
Gomes, S., Raimundo, L., Soares, J., Loureiro, J.B., Leão, M., Ramos, H., Monteiro, M.N., Lemos, A., Moreira, J., Pinto, M., Chlapek, P., Veselska, R., Sousa, E., Saraiva, L., 2019. New inhibitor of the TAp73 interaction with MDM2 and mutant p53 with promising antitumor activity against neuroblastoma. Cancer Lett. 446, 90–102. https://doi.org/10.1016/J.CANLET.2019.01.014.
Gordon, E., Schimmel, L., Frye, M., 2020. The importance of mechanical forces for in vitro endothelial cell biology. Front. Physiol. 11, 538479. https://doi.org/10.3389/FPHYS.2020.00684/PDF.
Gu, L., Zhang, H., He, J., Li, J., Huang, M., Zhou, M., 2011. MDM2 regulates MYCN mRNA stabilization and translation in human neuroblastoma cells. Oncogene 31 (11), 1342–1353. https://doi.org/10.1038/onc.2011.343.
Harapin, J., Börmel, M., Sapra, K.T., Brunner, D., Kaech, A., Medalia, O., 2015. Structural analysis of multicellular organisms with cryo-electron tomography. Nat. Methods 12 (7), 634–636. https://doi.org/10.1038/nmeth.3401.
Hatzi, E., Murphy, C., Zoephel, A., Ahorn, H., Tontsch, U., Bamberger, A.M., Yamauchi-Takihara, K., Schweigerer, L., Fotsis, T., 2002. N-myc oncogene overexpression down-regulates leukemia inhibitory factor in neuroblastoma. Eur. J. Biochem. 269, 3732–3741. https://doi.org/10.1046/J.1432-1033.2002.03066.X.
He, J., Gu, L., Zhang, H., Zhou, M., 2011. Crosstalk between MYCN and MDM2-p53 signal pathways regulates tumor cell growth and apoptosis in neuroblastoma. Cell Cycle 10, 2994–3002. https://doi.org/10.4161/CC.10.17.17118.
Hee, E., Wong, M.K., Tan, S.H., Choo, Z., Kuick, C.H., Ling, S., Yong, M.H., Jain, S., Lian, D.W.Q., Ng, E.H.Q., Yong, Y.F.L., Ren, M.H., Syed Sulaiman, N., Low, S.Y.Y., Chua, Y.W., Syed, M.F., Lim, T.K.H., Soh, S.Y., Iyer, P., Seng, M.S.F., Lam, J.C.M., Tan, E.E.K., Chan, M.Y., Tan, A.M., Chen, Y., Chen, Z., Chang, K.T.E., Loh, A.H.P., 2020. Neuroblastoma patient-derived cultures are enriched for a mesenchymal gene signature and reflect individual drug response. Cancer Sci. 111, 3780–3792. https://doi.org/10.1111/CAS.14610.
Horvilleur, E., Bauer, M., Goldschneider, D., Mergui, X., De la motte, A., Bénard, J., Douc-rasy, S., Cappellen, D., 2008. p73α isoforms drive opposite transcriptional and post-transcriptional regulation of MYCN expression in neuroblastoma cells. Nucleic Acids Res. 36, 4222–4232. https://doi.org/10.1093/NAR/GKN394.
Huang, M., Weiss, W.A., 2013. Neuroblastoma and MYCN. Cold Spring Harb. Perspect. Med. 3, a014415. https://doi.org/10.1101/cshperspect.a014415.
Ichimiya, S., Nakagawara, A., Sakuma, Y., Kimura, S., Ikeda, T., Satoh, M., Takahashi, N., Sato, N., Mori, M., 2000. p73: structure and function. Pathol. Int. 50, 589–593. https://doi.org/10.1046/J.1440-1827.2000.01090.X.
Inamori, K.I., Gu, J., Ohira, M., Kawasaki, A., Nakamura, Y., Nakagawa, T., Kondo, A., Miyoshi, E., Nakagawara, A., Taniguchi, N., 2006. High expression of N-acetylglucosaminyltransferase V in favorable neuroblastomas: involvement of its effect on apoptosis. FEBS Lett. 580, 627–632. https://doi.org/10.1016/J.FEBSLET.2005.12.089.
Iraci, N., Diolaiti, D., Papa, A., Porro, A., Valli, E., Gherardi, S., Herold, S., Eilers, M., Bernardoni, R., Della Valle, G., Perini, G., 2011. A SP1/MIZ1/MYCN repression complex recruits HDAC1 at the TRKA and p75NTR promoters and affects neuroblastoma malignancy by inhibiting the cell response to NGF. Cancer Res. 71, 404–412. https://doi.org/10.1158/0008-5472.CAN-10-2627/649607.
Jaghoori, M.M., Bleijlevens, B., Olabarriaga, S.D., 2016. 1001 ways to run AutoDock Vina for virtual screening. J. Comput. Aided Mol. Des. 30, 237–249. https://doi.org/10.1007/S10822-016-9900-9.
Jain, A., Lokhande, K.B., Singh, A., 2024. Breaking the "undruggable" barrier: revealing molecular mechanisms in Aurora Kinase A/Myc protein interplay targeting cancers. Med. Hypotheses 185, 111320. https://doi.org/10.1016/J.MEHY.2024.111320.
Kamińska, K., Szczylik, C., Bielecka, Z.F., Bartnik, E., Porta, C., Lian, F., Czarnecka, A.M., 2015. The role of the cell–cell interactions in cancer progression. J. Cell Mol. Med. 19, 283–296. https://doi.org/10.1111/JCMM.12408.
Lamouille, S., Xu, J., Derynck, R., 2014. Molecular mechanisms of epithelial-mesenchymal transition. Nat. Rev. Mol. Cell Biol. 15, 178–196. https://doi.org/10.1038/NRM3758.
Leão, M., Gomes, S., Bessa, C., Soares, J., Raimundo, L., Monti, P., Fronza, G., Pereira, C., Saraiva, L., 2015. Studying p53 family proteins in yeast: induction of autophagic cell death and modulation by interactors and small molecules. Exp. Cell Res. 330, 164–177. https://doi.org/10.1016/J.YEXCR.2014.09.028.
Li, C., Feng, C., Chen, Y., Wu, P., Li, P., Xiong, X., Peng, X., Wang, Z., Li, Y., 2022. Arsenic trioxide induces the differentiation of retinoic acid-resistant neuroblastoma cells via upregulation of HoxC9. Adv. Clin. Exp. Med. 31. https://doi.org/10.17219/ACEM/147463.
Li, Y., Prives, C., 2007. Are interactions with p63 and p73 involved in mutant p53 gain of oncogenic function? Oncogene 26 (15), 2220–2225. https://doi.org/10.1038/sj.onc.1210311.
Lin, L., Miao, L., Lin, H., Cheng, J., Li, M., Zhuo, Z., He, J., 2022. Targeting RAS in neuroblastoma: is it possible? Pharmacol. Ther. 236, 108054. https://doi.org/10.1016/J.PHARMTHERA.2021.108054.
Liu, Z., Chen, S.S., Clarke, S., Veschi, V., Thiele, C.J., 2021. Targeting MYCN in pediatric and adult cancers. Front. Oncol. 10, 623679. https://doi.org/10.3389/FONC.2020.623679.
Lundberg, K.I., Treis, D., Johnsen, J.I., 2022. Neuroblastoma heterogeneity, plasticity, and emerging therapies. Curr. Oncol. Rep. 24, 1053–1062. https://doi.org/10.1007/s11912-022-01270-8.
Ma, B., Pan, Y., Gunasekaran, K., Keskin, O., Venkataraghavan, R.B., Levine, A.J., Nussinov, R., 2005. The contribution of the Trp/Met/Phe residues to physical interactions of p53 with cellular proteins. Phys. Biol. 2, S56. https://doi.org/10.1088/1478-3975/2/2/S06.
Machado-Silva, A., Perrier, S., Bourdon, J.C., 2010. p53 family members in cancer diagnosis and treatment. Semin. Cancer Biol. 20, 57–62. https://doi.org/10.1016/j.semcancer.2010.02.005.
Matthay, K.K., Maris, J.M., Schleiermacher, G., Nakagawara, A., Mackall, C.L., Diller, L., Weiss, W.A., 2016. Neuroblastoma. Nat. Rev. Dis. Primers 2 (1), 1–21. https://doi.org/10.1038/nrdp.2016.78.
Matthay, K.K., Villablanca, J.G., Seeger, R.C., Stram, D.O., Harris, R.E., Ramsay, N.K., Swift, P., Shimada, H., Black, C.T., Brodeur, G.M., Gerbing, R.B., Reynolds, C.P., 1999. Treatment of high-risk neuroblastoma with intensive chemotherapy, radiotherapy, autologous bone marrow transplantation, and 13- cis -Retinoic acid. N. Engl. J. Med. 341, 1165–1173. https://doi.org/10.1056/NEJM199910143411601.
Meng, J., Tagalakis, A.D., Hart, S.L., 2020. Silencing E3 Ubiqutin ligase ITCH as a potential therapy to enhance chemotherapy efficacy in p53 mutant neuroblastoma cells. Sci. Rep. 10 (1), 1–12. https://doi.org/10.1038/s41598-020-57854-6, 2020.
Mlakar, V., Morel, E., Mlakar, S.J., Ansari, M., Gumy-Pause, F., 2021. A review of the biological and clinical implications of RAS-MAPK pathway alterations in neuroblastoma. J. Exp. Clin. Cancer Res. 40 (1), 1–16. https://doi.org/10.1186/S13046-021-01967-X, 2021.
Molenaar, J.J., Koster, J., Zwijnenburg, D.A., Van Sluis, P., Valentijn, L.J., Van Der Ploeg, I., Hamdi, M., Van Nes, J., Westerman, B.A., Van Arkel, J., Ebus, M.E., Haneveld, F., Lakeman, A., Schild, L., Molenaar, P., Stroeken, P., Van Noesel, M.M., Øra, I., Santo, E.E., Caron, H.N., Westerhout, E.M., Versteeg, R., 2012. Sequencing of neuroblastoma identifies chromothripsis and defects in neuritogenesis genes. Nature 483, 589–593. https://doi.org/10.1038/NATURE10910.
Murphy, C.M., O'Brien, F.J., Little, D.G., Schindeler, A., 2013. Cell-scaffold interactions in the bone tissue engineering triad. Eur. Cell. Mater. 26, 120–132. https://doi.org/10.22203/ECM.V026A09.
Nakagawara, A., Li, Y., Izumi, H., Muramori, K., Inada, H., Nishi, M., 2018. Neuroblastoma. Jpn. J. Clin. Oncol. 48, 214–241. https://doi.org/10.1093/jjco/hyx176.
Nakamura, M., Matsuo, T., Stauffer, J., Neckers, L., Thiele, C.J., 2003. Retinoic acid decreases targeting of p27 for degradation via an N-myc-dependent decrease in p27 phosphorylation and an N-myc-independent decrease in Skp2. Cell Death Differ. 10 (2), 230–239. https://doi.org/10.1038/sj.cdd.4401125, 2003.
Nicolai, S., Pieraccioli, M., Peschiaroli, A., Melino, G., Raschellà, G., 2015. Neuroblastoma: oncogenic mechanisms and therapeutic exploitation of necroptosis. Cell Death Dis. 6 (12). https://doi.org/10.1038/cddis.2015.354 e2010–e2010.
Nieto, M.A., Huang, R.Y.Y.J., Jackson, R.A.A., Thiery, J.P.P., 2016. EMT: 2016. Cell 166, 21–45. https://doi.org/10.1016/J.CELL.2016.06.028.

Nikolaev, A.Y., Li, M., Puskas, N., Qin, J., Gu, W., 2003. Parc: a cytoplasmic anchor for p53. Cell 112, 29–40. https://doi.org/10.1016/S0092-8674(02)01255-2/ATTACHMENT/7121D269-8353-4A66-B1A4-E5A7F5B58A41/MMC4.JPG.

Osterburg, C., Dötsch, V., 2022. Structural diversity of p63 and p73 isoforms. Cell Death Differ. 29 (5), 921–937. https://doi.org/10.1038/s41418-022-00975-4.

Otte, J., Dyberg, C., Pepich, A., Johnsen, J.I., 2021. MYCN function in neuroblastoma development. Front. Oncol. 10, 624079. https://doi.org/10.3389/FONC.2020.624079.

Park, J.R., Eggert, A., Caron, H., 2010. Neuroblastoma: biology, prognosis, and treatment. Hematol. Oncol. Clin. N. Am. 24, 65–86. https://doi.org/10.1016/J.HOC.2009.11.011.

Pinto, N.R., Applebaum, M.A., Volchenboum, S.L., Matthay, K.K., London, W.B., Ambros, P.F., Nakagawara, A., Berthold, F., Schleiermacher, G., Park, J.R., Valteau-Couanet, D., Pearson, A.D.J., Cohn, S.L., 2015. Advances in risk classification and treatment strategies for neuroblastoma. J. Clin. Oncol. 33, 3008–3017. https://doi.org/10.1200/JCO.2014.59.4648.

Powell, E., Piwnica-Worms, D., Piwnica-Worms, H., 2014. Contribution of p53 to metastasis. Cancer Discov. 4, 405–414. https://doi.org/10.1158/2159-8290.CD-13-0136.

Pucci, P., Lee, L.C., Han, M., Matthews, J.D., Jahangiri, L., Schlederer, M., Manners, E., Sorby-Adams, A., Kaggie, J., Trigg, R.M., Steel, C., Hare, L., James, E.R., Prokoph, N., Ducray, S.P., Merkel, O., Rifatbegovic, F., Luo, J., Taschner-Mandl, S., Kenner, L., Burke, G.A.A., Turner, S.D., 2024. Targeting NRAS via miR-1304-5p or farnesyltransferase inhibition confers sensitivity to ALK inhibitors in ALK-mutant neuroblastoma. Nat. Commun. 15 (1), 1–19. https://doi.org/10.1038/s41467-024-47771-x.

Raimundo, L., Espadinha, M., Soares, J., Loureiro, J.B., Alves, M.G., Santos, M.M.M., Saraiva, L., 2018. Improving anticancer activity towards colon cancer cells with a new p53-activating agent. Br. J. Pharmacol. 175, 3947–3962. https://doi.org/10.1111/BPH.14468.

Raj, N., Attardi, L.D., 2017. The transactivation domains of the p53 protein. Cold Spring Harb. Perspect. Med. 7, a026047. https://doi.org/10.1101/CSHPERSPECT.A026047.

Ramos, H., Raimundo, L., Saraiva, L., 2020. p73: from the p53 shadow to a major pharmacological target in anticancer therapy. Pharmacol. Res. 162, 105245. https://doi.org/10.1016/j.phrs.2020.105245.

Resende, D.I.S.P., Durães, F., Maia, M., Sousa, E., Pinto, M.M.M., 2020a. Recent advances in the synthesis of xanthones and azaxanthones. Org. Chem. Front. 7, 3027–3066. https://doi.org/10.1039/D0QO00659A.

Resende, D.I.S.P., Pereira-Terra, P., Inácio, Â.S., Da Costa, P.M., Pinto, E., Sousa, E., Pinto, M.M.M., 2018. Lichen xanthones as models for new antifungal agents. Molecules 23. https://doi.org/10.3390/MOLECULES23102617. Page 2617 23, 2617.

Resende, D.I.S.P., Pereira-Terra, P., Moreira, J., Freitas-Silva, J., Lemos, A., Gales, L., Pinto, E., de Sousa, M.E., da Costa, P.M., Pinto, M.M.M., 2020b. Synthesis of a small Library of nature-inspired xanthones and Study of their antimicrobial activity. Molecules 25. https://doi.org/10.3390/MOLECULES25102405. Page 2405 25, 2405.

Schwab, M., Alitalo, K., Klempnauer, K.H., Varmus, H.E., Bishop, J.M., Gilbert, F., Brodeur, G., Goldstein, M., Trent, J., 1983. Amplified DNA with limited homology to myc cellular oncogene is shared by human neuroblastoma cell lines and a neuroblastoma tumour. Nature 305 (5931), 245–248. https://doi.org/10.1038/305245a0.

Schwab, M., Ellison, J., Buschf, M., Rosenaut, W., Varmust, H.E., Michael Bishop, J., Hooper, G.W., 1984. Enhanced expression of the human gene N-myc consequent to amplification of DNA may contribute to malignant progression of neuroblastoma. Proc. Natl. Acad. Sci. 81, 4940–4944. https://doi.org/10.1073/PNAS.81.15.4940.

Seeger, R.C., Brodeur, G.M., Sather, H., Dalton, A., Siegel, S.E., Wong, K.Y., Hammond, D., 1985. Association of multiple copies of the N-myc oncogene with rapid progression of neuroblastomas. N. Engl. J. Med. 313, 1111–1116. https://doi.org/10.1056/NEJM198510313131802.

Seeliger, D., De Groot, B.L., 2010. Ligand docking and binding site analysis with PyMOL and Autodock/Vina. J. Comput. Aided Mol. Des. 24, 417–422. https://doi.org/10.1007/s10822-010-9352-6.

Shi, X., Wang, Y., Zhang, L., Zhao, W., Dai, X., Yang, Y.G., Zhang, X., 2022. Targeting bromodomain and extra-terminal proteins to inhibit neuroblastoma tumorigenesis through regulating MYCN. Front. Cell Dev. Biol. 10, 1021820. https://doi.org/10.3389/fcell.2022.1021820.

Shi, Y., Takenobu, H., Kurata, K., Yamaguchi, Y., Yanagisawa, R., Ohira, M., Koike, K., Nakagawara, A., Jiang, L.L., Kamijo, T., 2010. HDM2 impairs Noxa transcription and affects apoptotic cell death in a p53/p73-dependent manner in neuroblastoma. Eur. J. Cancer 46, 2324–2334. https://doi.org/10.1016/j.ejca.2010.05.026.

Slack, A., Chen, Z., Tonelli, R., Pule, M., Hunt, L., Pession, A., Shohet, J.M., 2005. The p53 regulatory gene MDM2 is a direct transcriptional target of MYCN in neuroblastoma. Proc. Natl. Acad. Sci. U. S. A. 102, 731–736. https://doi.org/10.1073/pnas.0405495102.

Soares, J., Espadinha, M., Raimundo, L., Ramos, H., Gomes, A.S., Gomes, S., Loureiro, J. B., Inga, A., Reis, F., Gomes, C., Santos, M.M.M., Saraiva, L., 2017. DIMP53-1: a novel small-molecule dual inhibitor of p53–MDM2/X interactions with multifunctional p53-dependent anticancer properties. Mol. Oncol. 11, 612–627. https://doi.org/10.1002/1878-0261.12051.

Soares, J., Raimundo, L., Pereira, N.A.L., Monteiro, Â., Gomes, S., Bessa, C., Pereira, C., Queiroz, G., Bisio, A., Fernandes, J., Gomes, C., Reis, F., Gonçalves, J., Inga, A., Santos, M.M.M., Saraiva, L., 2016. Reactivation of wild-type and mutant p53 by tryptophanol-derived oxazoloisoindolinone SLMP53-1, a novel anticancer small-molecule. Oncotarget 7, 4326–4343. https://doi.org/10.18632/oncotarget.6775.

Stindt, M.H., Muller, P.A.J., Ludwig, R.L., Kehrloesser, S., Dötsch, V., Vousden, K.H., 2014. Functional interplay between MDM2, p63/p73 and mutant p53. Oncogene 34 (33), 4300–4310. https://doi.org/10.1038/onc.2014.359.

Tao, T., Shi, H., Mariani, L., Abraham, B.J., Durbin, A.D., Zimmerman, M.W., Powers, J. T., Missios, P., Ross, K.N., Perez-Atayde, A.R., Bulyk, M.L., Young, R.A., Daley, G.Q., Thomas Look, A., 2020. LIN28B regulates transcription and potentiates MYCN-induced neuroblastoma through binding to ZNF143 at target gene promotors. Proc. Natl. Acad. Sci. U. S. A. 117, 16516–16526. https://doi.org/10.1073/PNAS.1922692117.

Van Maerken, T., Speleman, F., Vermeulen, J., Lambertz, I., De Clercq, S., De Smet, E., Yigit, N., Coppens, V., Philippé, J., De Paepe, A., Marine, J.C., Vandesompele, J., 2006. Small-Molecule MDM2 antagonists as a new therapy concept for neuroblastoma. Cancer Res. 66, 9646–9655. https://doi.org/10.1158/0008-5472.CAN-06-0792.

Vilgelm, A., El-Rifai, W., Zaika, A., 2008. Therapeutic prospects for p73 and p63: rising from the shadow of p53. Drug Resist. Updates 11, 152–163. https://doi.org/10.1016/J.DRUP.2008.08.001.

Villasante, A., Corominas, J., Alcon, C., Garcia-Lizarribar, A., Mora, J., Lopez-Fanarraga, M., Samitier, J., 2024. Identification of GB3 as a novel biomarker of tumor-derived vasculature in neuroblastoma using a stiffness-based model. Cancers (Basel) 16, 1060. https://doi.org/10.3390/CANCERS16051060/S1.

Vousden, K.H., Lane, D.P., 2007. p53 in health and disease. Nat. Rev. Mol. Cell Biol. 8 (8), 275–283. https://doi.org/10.1038/nrm2147.

Wang, C., Teo, C.R., Sabapathy, K., 2020. p53-Related transcription targets of TAp73 in cancer Cells—Bona fide or distorted reality? Int. J. Mol. Sci. 21. https://doi.org/10.3390/ijms21041346. Page 1346 21, 1346.

Wang, H., Guo, M., Wei, H., Chen, Y., 2023. Targeting p53 pathways: mechanisms, structures and advances in therapy. Signal Transduct. Targeted Ther. 8 (1), 1–35. https://doi.org/10.1038/s41392-023-01347-1.

Wang, Y., Gao, S., Wang, W., Xia, Y., Liang, J., 2018. Downregulation of N-Myc inhibits neuroblastoma cell growth via the Wnt/β-catenin signaling pathway. Mol. Med. Rep. 1, 377–384. https://doi.org/10.3892/mmr.2018.8966.

Wells, M., Tidow, H., Rutherford, T.J., Markwick, P., Jensen, M.R., Mylonas, E., Svergun, D.I., Blackledge, M., Fersht, A.R., 2008. Structure of tumor suppressor p53 and its intrinsically disordered N-terminal transactivation domain. Proc. Natl. Acad. Sci. U. S. A. 105, 5762–5767. https://doi.org/10.1073/pnas.0801353105.

Xue, C., Zhang, T., Xie, X., Zhang, Q., Zhang, S., Zhu, B., Lin, Y., Cai, X., 2017. Substrate stiffness regulates arterial-venous differentiation of endothelial progenitor cells via the Ras/Mek pathway. Biochim. Biophys. Acta Mol. Cell Res. 1864, 1799–1808. https://doi.org/10.1016/J.BBAMCR.2017.07.006.

Yammine, A., Gao, J., Kwan, A.H., 2019. Tryptophan fluorescence quenching assays for measuring protein-ligand binding affinities: principles and a practical guide. Bio Protoc 9, e3253. https://doi.org/10.21769/BIOPROTOC.3253.

Zacharioudakis, E., Gavathiotis, E., 2022. Targeting protein conformations with small molecules to control protein complexes. Trends Biochem. Sci. 47, 1023–1037. https://doi.org/10.1016/j.tibs.2022.07.002.

Zafar, A., Wang, W., Liu, G., Xian, W., McKeon, F., Zhou, J., Zhang, R., 2021. Targeting the p53-MDM2 pathway for neuroblastoma therapy: rays of hope. Cancer Lett. 496, 16–29. https://doi.org/10.1016/J.CANLET.2020.09.023.

Zhang, M., Zhang, B., 2025. Extracellular matrix stiffness: mechanisms in tumor progression and therapeutic potential in cancer. Exp. Hematol. Oncol. 14 (1), 1–34. https://doi.org/10.1186/S40164-025-00647-2.

Zhou, X., Wang, X., Li, N., Guo, Y., Yang, X., Lei, Y., 2023. Therapy resistance in neuroblastoma: mechanisms and reversal strategies. Front. Pharmacol. 14, 1114295. https://doi.org/10.3389/FPHAR.2023.1114295.

Zhu, X., Wimmer, K., Kuick, R., Lamb, B.J., Motyka, S., Jasty, R., Castle, V.P., Hanash, S. M., 2002. N-myc modulates expression of p73 in Neuroblastoma. Neoplasia 4, 432–439. https://doi.org/10.1038/SJ.NEO.7900255.

Zingales, V., Esposito, M.R., Quagliata, M., Cimetta, E., Ruiz, M.J., 2024. Comparative Study of spheroids (3D) and monolayer cultures (2D) for the In vitro assessment of cytotoxicity induced by the mycotoxins Sterigmatocystin, Ochratoxin A and patulin. Foods 13, 564. https://doi.org/10.3390/FOODS13040564/S1.